

End-to-end Optimization of Single-Shot Quantum Machine Learning for Bayesian Inference

Theodoros Ilias,¹ Fangjun Hu,¹ Marti Vives,¹ and Hakan E. Türeci^{1,*}

¹*Department of Electrical and Computer Engineering,
Princeton University, Princeton, NJ 08544, USA*

We introduce an end-to-end optimization strategy for quantum machine learning that directly targets performance under finite measurement resources, where learning objectives are defined directly at the level of task performance. The method is applied on a Bayesian quantum metrology task since it provides a natural testbed with known fundamental limits and scaling with system size. The sampling-aware hybrid algorithm achieves a single-shot risk within 1 dB of the -20 dB Bayesian limit using 32 qubits. We extend the Bayesian framework from parameter estimation to global function inference, where the task is to infer a target function of the sensor input drawn from an arbitrary prior, and we demonstrate a clear computational-sensing advantage for direct functional inference over indirect reconstruction. We relate the corresponding Bayesian risk to the Capacity metric and argue that the Resolvable Expressive Capacity provides a natural measure of the space of functions accessible in a single shot. The resulting eigentask analysis identifies noise-robust feature combinations that yield compact estimators with improved accuracy and reduced optimization cost in resource-limited or real-time on-device settings.

I. INTRODUCTION

Training and inference on quantum hardware are fundamentally constrained by finite coherence times, limited measurement resources, restricted physical encodings, and unavoidable mismatch between hardware behavior and idealized numerical models. In this work, we focus specifically on the limitations imposed by finite sampling, which constitute a dominant and inescapable bottleneck for near-term quantum machine learning. A common approach in quantum machine learning (QML) is to optimize a target loss under idealized, effectively infinite-shot assumptions, and only subsequently assess performance when a finite number of measurements is imposed. This separation has two key drawbacks. First, as is now well appreciated [1], it obscures the true hardware cost of implementation: models that are optimal in the infinite-sampling limit may demand prohibitively large shot budgets to deliver that performance, severely limiting their practical usefulness. Second, and more subtly, the structure of the optimization problem itself can change qualitatively under finite measurement resources, so that solutions found in the idealized limit need not be reachable or optimal when sampling is constrained. While recent work has shown that finite-shot noise can, in some cases, act as a stochastic regularizer that assists gradient-based optimization [2], this perspective still treats sampling noise as incidental rather than foundational. Here, we instead adopt an end-to-end approach in which the estimator, training dynamics, and inference procedure are explicitly optimized for a fixed and finite sampling budget. By performing optimization directly on the quantum device and treating the hardware as a noisy input–output map, we develop a quantum

machine learning framework whose performance is intrinsically matched to realistic experimental constraints, rather than extrapolated from an idealized limit.

Our approach builds on recent developments in physical neural network (PNN) theory [3, 4] and adapts them to the optimization of qubit-based devices under strict measurement constraints. Within the PNN view, the device is treated as a black box whose resolvable output functions can be characterized directly through sampling. This perspective also directly addresses model–hardware mismatch: the optimal estimators are defined by the actual device and measurement conditions, rather than by an idealized numerical surrogate.

In QML applications, a central challenge in evaluating the advantage conferred by the use of a quantum substrate over a classical one lies in the absence of a systematic framework to determine the fundamental limit allowed by quantum mechanics. Equally important is a methodology for systematically comparing its performance to that of a classical substrate under equivalent resource constraints. We find that the application of a QML-based framework to bayesian quantum metrology (BQM) offers a rigorous basis to address such challenge because of (1) the existence of a cost function for which the scaling behavior and performance with system size can be derived and computed, and (2) a comparative analysis can in principle be conducted with respect to the equivalent class of sensors operating in the classical limit. We present one approach here that applies this general strategy.

From the perspective of quantum metrology, a PNN-based approach provides a data-driven methodology that adapts naturally to the control and measurement resources of a given physical sensor. Limitations in accessible resource states, available Hamiltonian interactions, and readout fidelity often create bottlenecks that require sophisticated techniques to approach Heisenberg scaling [5–7], the ultimate limit accessible through lin-

* tureci@princeton.edu

ear quantum measurements, as demonstrated in recent work utilizing collective-state protocols without single-particle detection [8], squeezed superradiance-based readout schemes [9], and scrambling-enhanced metrology [10]. A PNN framework provides a complementary route by optimizing directly within the device’s physical constraints, using the data generated by the sensor as it samples the signal. The effectiveness of such an approach has been demonstrated with variational quantum metrology [11, 12], that have the utility for both preparing metrologically-useful entangled resource states, and also in producing decoders that are able to effectively concentrate the parameter-dependence of the entangled state into simple observables that can be easily measured. A recent experiment provided a proof-of-principle demonstration in a trapped-ion platform that this approach can be highly effective [13].

The task considered here is to train a parametrized circuit to estimate a target function, $f^*(u)$, of an input phase variable u in a single measurement. The input is drawn from a prior distribution, $p(u)$, and the cost function maximizes the accuracy of the inferred function value. This formulation extends Bayesian quantum metrology [11–13] to global function estimation under arbitrary priors, a task we refer to as Bayesian quantum inference (BQI).

A principled comparison across physical substrates requires a metric that quantifies the space of functions that can be resolved with fixed resources. The Resolvable Expressive Capacity (REC) introduced in Ref. [3] provides such a measure. For a single-shot budget it reduces, for linear function targets and Gaussian priors, to the Bayesian mean-square error used in single-parameter metrology [11, 13]. REC therefore offers a natural extension of this metric to the broader BQI setting. For qubit-based systems with projective measurements, REC admits a tight analytic bound [3]. A spectral analysis of REC identifies eigentasks, the functions that can be approximated with the highest signal-to-noise ratio [3]. These provide the smallest latent space of effective features and can drastically reduce the optimization burden compared to working in the exponentially large full feature space.

The measurement-driven optimization of sensor parameters for single-shot estimation is expected to be a challenging problem. In the asymptotic limit of infinite measurement shots, where output features converge to their quantum expectation values and sampling noise vanishes, gradient-based variational QML approaches have been shown to scale poorly due to vanishing gradients [14], rendering gradient-based training practically ineffective due to the finite number of experiments that can be practically performed. Although circuit expressivity theoretically increases with depth [15–18], the optimization landscape of sufficiently deep parameterized quantum circuits exhibits exponentially vanishing gradients, leading to the well-known barren plateau phenomenon [14]. These results have driven research into the

adoption of gradient-free hybrid optimization methods. A class of QML algorithms well suited to NISQ devices that avoids the optimization challenges of variational approaches is quantum reservoir computing (QRC) [19–24]. When combined with mid-circuit feature extraction under finite-shot constraints, QRC can address limitations imposed by finite coherence times, as demonstrated by the NISQRC algorithm [4].

In QRC, an untrained quantum system serves as a high-dimensional nonlinear feature generator. Its fixed dynamics transform input data into a rich set of observables. A linear estimator in this space of non-linear features is optimized on labeled training data. Because only the classical weights are trained, a convex optimization efficiently solvable via standard linear algebra routines such as SVD, training requires far fewer quantum evaluations and avoids the vanishing-gradient issues that hinder variational approaches. Recent experimental demonstrations using atom-based reservoirs (108 qubits) [25] and Gaussian boson samplers (8176 [26] and 400 [27] modes, respectively), have highlighted the potential for scalability of this approach. However, these studies also report a rapid loss in accuracy when the sampling is reduced [23, 28, 29]. Going beyond these studies, and while retaining the simplicity of a reservoir-inspired estimator, we show that optimizing the internal parameters under finite-shot conditions yields dramatically improved accuracy and reduces measurement requirements down to the single-shot level for the BQI tasks considered. We conjecture that, for the class of circuits considered, the optimal BQI sensor remains robust under on-device optimization.

To this end, we introduce a sampling-aware, end-to-end hybrid optimization algorithm for single-shot BQI in which state preparation, encoding, measurement, and classical post-processing are optimized jointly. This unified treatment contrasts with approaches that analyze performance through Fisher-information bounds [30–32], focus primarily on the design of probe states [33–35], or optimize the final measurement [36–40]. These perspectives often address individual elements of the sensing pipeline, whereas our framework directly targets the overall inference task and the estimator that ultimately determines performance in the single-shot regime. Applied to a single-parameter metrology task, the proposed method reaches a risk of -19.1 dB with 32 qubits, close to the -20 dB limit achieved by the optimal Bayesian sensor under the same resources [41]. Unlike that optimal sensor, our circuit depth is fixed throughout the optimization.

Recent work has introduced the concept of a quantum computational-sensing advantage [42, 43], referring to potential performance gains achieved when quantum sensors are integrated with on-device quantum information processing to perform part of the inference task directly. Importantly, this notion of advantage does not rely on reaching system scales where classical computation of equivalent accuracy becomes intractable. Here, we propose quantitative way to assess such comparative advan-

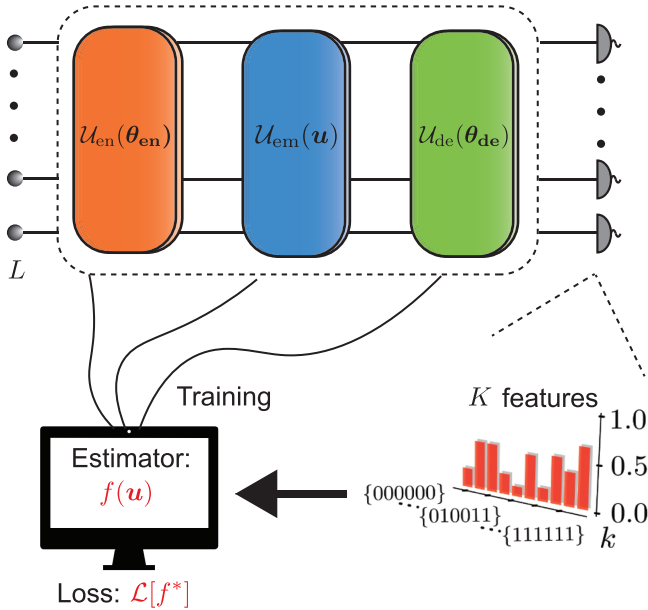


Figure 1. Physical neural network approach to quantum sensing. L initially uncorrelated qubits are prepared in a metrologically useful state $\rho_{\text{en}} = \mathcal{U}_{\text{en}}(\theta_{\text{en}})\rho_0$ via a parameterized entangling superoperator $\mathcal{U}_{\text{en}}(\theta_{\text{en}})$. In turn, the signal input \mathbf{u} , drawn from a training dataset, is embedded on the quantum system. A parameterized decoder $\mathcal{U}_{\text{de}}(\theta_{\text{de}})$ is applied to the encoded state, followed by projective measurements in the computational basis. Collecting the measurement features allows to construct an estimation $f(\mathbf{u})$ of the target function $f^*(\mathbf{u})$ and calculate the objective loss function. Optimizing such loss function allow us to train the internal parameter of the quantum circuit as well as the estimator enabling the optimization of the whole sensing pipeline. We note that although our framework places no restriction on the form of the entangling, embedding and decoding operations and allows them to be arbitrary quantum maps, in present work we focus on unitary implementations.

tage based on the Bayesian risk under identical resource constraints: (i) a quantum sensor optimized to estimate a latent parameter, followed by classical post-processing to compute a desired function of that parameter; and (ii) a quantum sensor optimized end-to-end to infer that function directly in a single shot. The corresponding Bayesian risks for a 32-qubit system are found to be -2.9 dB in scenario (i) versus -4.7 dB in scenario (ii), respectively – a statistically significant improvement that illustrates how direct functional optimization, i.e. BQI, can realize a measurable computational-sensing benefit.

The rest of the paper is organized as follows. In Section II A we review the conceptual foundations of BQM while Section II B presents the general framework of our quantum computation sensing approach and establishes its connection to the Resolvable Expressive Capacity (REC) introduced in Ref. [11] for finite-sample scenarios. In Section II C, we detail an efficient optimization procedure that is essential for the successful end-to-end train-

ing of the sensing pipeline. Section II E 1 introduces the concept of eigentask learning, while Section II provides several illustrative examples of approximating functions of inputs drawn from various probability distributions, thereby highlighting the versatility and advantages of our approach. Finally, Section III summarizes our findings and outlines potential directions for future research.

II. THEORY & RESULTS

A. Review of Bayesian Quantum Metrology

Here, we review the conceptual foundations of BQM for single-parameter estimation [11, 13], introduce the cost function appropriate to an arbitrary given experimental setting, and review known results on optimal sensor configurations and metrological bounds imposed by quantum theory. This sets the stage for extending the framework in the next section to global function estimation under arbitrary priors. Because the cost function must be tied to a concrete metrological task, we focus on Ramsey interferometry, where optimality is defined by achieving the maximum single-shot SNR for phase estimation.

Consider the estimation of a phase u imparted by a weak electromagnetic pulse on a qubit-based sensor system composed of L qubits. The pulse whose properties one wants to estimate encodes a phase in the sensor by evolving to the state $\rho_u = \mathcal{U}_{\text{em}}(u)\rho_{\text{en}}$, where ρ_{en} is a prepared probe state and $\mathcal{U}_{\text{em}}(u) \equiv e^{-iu\hat{H}} \cdot e^{iu\hat{H}}$ the unitary embedding channel generated by \hat{H} and encodes the unknown phase u . Estimation of u is performed using measurement outcomes j , defined by a positive operator-valued measure (POVM) $\{\hat{M}_j\}_{j=1}^K$. Conditioned on the true value of u , outcome j occurs with probability $p(j|u) = x_j(u) = \text{tr} \{ \hat{M}_j \rho_u \}$. A natural metric of the performance of the estimation accuracy is the mean squared error (MSE) $\text{MSE}(u) = \sum_{j=1}^K (u - u_{\text{est}}(j))^2 p(j|u)$ with K being the number of the possible outcomes. Minimizing such a metric simultaneously for a wide range of phases u is impossible since probe states, POVMs and estimators that are optimal for some phase values might not work for some others [44]. Consequently, a more appropriate metric corresponds to the MSE averaged over the prior distribution of u , $p(u)$ that reflects the statistical properties of the unknown parameter suggests the use of BMSE, $\text{BMSE} = \int du p(u) \text{MSE}(u)$ [11].

Although lower bounds on the BMSE described above optimized over all possible probe states, estimators and POVMs together with the construction of an iterative numerical algorithm to find them has been studied in the past [41, 45, 46], it has only recently been shown that one can approach such bounds using shallow circuits composed of experimentally accessible gates, both in the single-parameter [11, 13] and multi-parameter [12] settings.

B. PNN approach to Global Function Sensing

In this section we present the six components of the quantum computational sensing framework. Each element is specified in detail because end-to-end optimization of the sensing pipeline requires a precise definition of every stage. Together these components form the architecture that enables end-to-end BQI in the quantum metrological setting examined later. The formulation below addresses the general case of an S -shot budget and high-dimensional inputs $\mathbf{u} = (u_1, \dots, u_d)$.

- 1. Training/Testing Dataset:** We assume access to a labeled dataset of size N_{tot} consisting of input–output pairs $\{\mathbf{u}_i, \mathbf{f}^*(\mathbf{u}_i)\}$, where $\mathbf{f}^* = (f_1, \dots, f_D)$ is the vector-valued target function to be learned and the inputs \mathbf{u} are sampled from a general prior distribution $p(\mathbf{u})$ with a compact support. Here, the vector-valued target function allows for multi-parameter estimation. Following the standard machine-learning paradigms, this dataset is randomly divided into a training set of size N_{tr} , used for optimizing the model parameters, and a testing set of size $N_{\text{ts}} = N_{\text{tot}} - N_{\text{tr}}$, used exclusively to evaluate the generalization performance of the trained model.
- 2. Entangled Probe Preparation:** The system is initialized in a fixed quantum state ρ_0 and subsequently transformed into a metrologically useful state $\rho_{\text{en}} = \mathcal{U}_{\text{en}}(\boldsymbol{\theta}_{\text{en}})\rho_0$ via a parameterized entangling superoperator $\mathcal{U}_{\text{en}}(\boldsymbol{\theta}_{\text{en}})$, where $\boldsymbol{\theta}_{\text{en}}$ denotes a set of tunable parameters. Henceforth, the calligraphic operators refer to superoperators defined as $\mathcal{U} \cdot U = U \cdot U^\dagger$.
- 3. Input Embedding:** The classical input \mathbf{u} is embedded into the quantum state using a parameter-dependent superoperator $\mathcal{U}_{\text{em}}(\mathbf{u})$, yielding the input-encoded state $\rho_{\text{em}}(\mathbf{u}) = \mathcal{U}_{\text{em}}(\mathbf{u})\rho_{\text{en}}$.
- 4. Decoding and Feature Extraction via Quantum Measurement:** A parameterized decoder $\mathcal{U}_{\text{de}}(\boldsymbol{\theta}_{\text{de}})$ is applied to the encoded state, followed by projective measurements in the computational basis. This measurement process realizes a positive operator-valued measure (POVM) $\{\hat{M}_j\}_{j=1}^K$, allowing access to information encoded in the final state

$$\rho(\mathbf{u}) = \mathcal{U}_{\text{de}}(\boldsymbol{\theta}_{\text{de}})\mathcal{U}_{\text{em}}(\mathbf{u})\mathcal{U}_{\text{en}}(\boldsymbol{\theta}_{\text{en}})\rho_0.$$

Performing S repeated measurements (shots) on this state yields a sequence of independent outcomes $\mathbf{j} = (j_1, j_2, \dots, j_S)$, from which we construct the empirical *feature vector* $\mathbf{X}(\mathbf{u}) = (X_1(\mathbf{u}), X_2(\mathbf{u}), \dots, X_K(\mathbf{u}))$ with $X_j = \frac{1}{S} \sum_s \delta(j_s - j)$. Thus X_j is the empirical S -shot frequency of outcome j and can be extracted from a physical device by performing S experiments for any

input \mathbf{u} sampled from $p(\mathbf{u})$ and vectorizing the histogram of outcomes (see Fig. 1). Equivalently, the parameters X_j correspond to the maximum-likelihood estimates of the categorical distribution over K outcomes, where the conditional probability of obtaining outcome j given the control \mathbf{u} is $p(j \mid \mathbf{u}) = x_j(\mathbf{u}) = \text{tr}\{\hat{M}_j \rho(\mathbf{u})\}$, as inferred from an S -shot measurement experiment.

In what follows, it will be useful to define the S -shot fluctuation vector by subtracting the expectation $X_j(\mathbf{u}) = x_j(\mathbf{u}) + \zeta_j(\mathbf{u})$, where now $\zeta_j(\mathbf{u})$ denotes a zero-mean stochastic fluctuation due to finite-sample (quantum shot) noise characterized with covariance $\text{Cov}[\zeta(\mathbf{u})] = \frac{1}{S}\boldsymbol{\Sigma}(\mathbf{u})$, where $\boldsymbol{\Sigma}(\mathbf{u}) = \text{diag}(\mathbf{x}(\mathbf{u})) - \mathbf{x}(\mathbf{u})\mathbf{x}(\mathbf{u})^T$. For additional details, see Ref. [3].

- 5. Estimator Construction and Training:** Given the measured features $\mathbf{X}(\mathbf{u})$, we approximate the target function using a linear estimator of the form

$$f_{\text{est},i}(\mathbf{u}) = \sum_{j=1}^K w_{ij} X_j(\mathbf{u}), \quad (1)$$

where w_{ij} is a learnable weight matrix with dimension $D \times K$. This estimator based on a complete set of POVMs was introduced in Ref. [3] for characterizing the function expression capacity of a given physical system under finite sampling of its projectively measured outputs. Here, we adopt this estimator because (1) it cleanly separates the non-linear action of the sensor embodied in its measured features $X_k(\mathbf{u})$ from a postprocessor that has a minimal action – a linear projection, and (2) because it allows the hardware-efficient training of the sensor parameters $(\boldsymbol{\theta}_{\text{en}}, \boldsymbol{\theta}_{\text{de}})$ through an optimization methodology we introduce in Section II C.

- 6. The Cost Function:** A key quantity of our analysis is the definition of the cost function which in general takes the form:

$$l[f^*] = \mathbb{E}_{\mathbf{u}}[\mathbb{E}[(\mathbf{f}^*(\mathbf{u}) - \mathbf{f}_{\text{est}}(\mathbf{u})) \cdot (\mathbf{f}^*(\mathbf{u}) - \mathbf{f}_{\text{est}}(\mathbf{u})) \mid \mathbf{u}]]. \quad (2)$$

Here, $\mathbb{E}_{\mathbf{u}}[g(\mathbf{u})] \equiv \int d\mathbf{u} p(\mathbf{u}) g(\mathbf{u})$ denotes the expectation over the input distribution $p(\mathbf{u})$, and $\mathbb{E}[\cdot \mid \mathbf{u}]$ represents the expectation over measurement outcomes. Note here the similarity of such quantity to the BMSE for the special case of $f^*(\mathbf{u}) = \mathbf{u}$. For S -shot sampling of POVM measurements with outcomes $\mathbf{j} = (j_1, j_2, \dots, j_S)$, it is formally defined by $\mathbb{E}[\cdot \mid \mathbf{u}] \equiv \sum_{\mathbf{j}} p(\mathbf{j} \mid \mathbf{u}) [\cdot]$. Here, the sum is taken over all possible S -measurement outcome vectors \mathbf{j} . If the measurements are independent of each other, $p(\mathbf{j} \mid \mathbf{u})$ only depends on the count vector $\mathbf{N}(\mathbf{j}) = (N_1, \dots, N_K)$ whose components are non-negative integers satisfying $\sum_{j=1}^K N_j = S$,

and $P(\mathbf{N}(\mathbf{j})|\mathbf{u}) = \frac{S!}{\prod_{j=1}^K N_j!} \prod_{j=1}^K p(j|\mathbf{u})^{N_j}$, where $p(j|\mathbf{u})$ is, as defined earlier through the Born rule, the probability of obtaining outcome j in an experimental run for the given input \mathbf{u} . Furthermore, adopting an estimator such as in Eq. (1) and minimizing the loss function with respect to the weight vector, \mathbf{w} , we arrive to the definition of the post reservoir loss function

$$\mathcal{L}(\boldsymbol{\theta}) = \min_{\mathbf{w} \in \mathbb{R}^K} l(\boldsymbol{\theta}, \mathbf{w}), \quad (3)$$

where $\boldsymbol{\theta}$ denotes all the internal parameters. The importance of such loss is further described in Sec. II C. Our framework naturally applies to functions $f : \mathbb{R}^d \rightarrow \mathbb{R}^D$, allowing for multi-parameter estimation and vector-valued targets. Consider for example estimating the scalar quantity $B_x^2 + B_y^2 + B_z^2$ from three field components (B_x, B_y, B_z) ; where here the input dimension is $d = 3$ and the output dimension is $D = 1$. In the remainder of this work, however, we focus on the scalar case $d = D = 1$, i.e., approximation of a single-parameter scalar function $f : \mathbb{R} \rightarrow \mathbb{R}$. Finally, in appendix A we show that in the special case of a single shot estimation ($S = 1$) of a scalar parameter u drawn from a Gaussian prior $p(u)$, the cost function coincides with the Bayesian MSE [47]

when the target function is chosen to be a linear function $f^*(u) = u$:

$$\mathcal{L}[f^*] \rightarrow \int du p(u) \sum_{j=1}^K p(j|u) (u - u_{\text{est}}(j))^2 \quad (4)$$

where the estimator is given by $u_{\text{est}}(j) = \sum_{\ell} w_{\ell} \delta_{\ell,j}$.

1. Single-parameter Metrology and Capacity

The cost function defined in Eq. (3) serves as the central performance metric in our data-driven sensing framework, quantifying how well the optimized sensing pipeline approximates a target function $f^*(u)$. Beyond the role as an optimization objective, we discuss in this section how this cost function can serve as a metric for characterizing the space of functions that a given sensor can resolve with the optimal estimator Eq. (1). The cost function Eq. (2) is linearly related to the *Capacity* $C[f^*]$ introduced in Ref. [3]

$$C[f^*] = 1 - \frac{\mathcal{L}[f^*]}{\mathbb{E}_{\mathbf{u}}[f^{*2}]} \quad (5)$$

Normalization over the prior here ensures that $0 \leq C \leq 1$. This connection brings out three important observations. First, given a sensor with internal parameters $(\boldsymbol{\theta}_{\text{en}}, \boldsymbol{\theta}_{\text{de}})$, a tight bound can be found for the total function expression capacity the sensor can resolve at S shots

through the estimator Eq. (1). This is a real number C_T that can be estimated by experimentally sampling the physical system constituting the sensor in its input space subject to the prior distribution $p(u)$. Second, a set of 2^L orthonormal functions $y^{(j)}$ can be constructed that have provably highest SNR at S shots. These results will be discussed in Sec. II D. Third, as we show in this section, when the prior is broad over the support of u , the capacity C serves as a global information-theoretic measure that, in the local limit, reduces to previously introduced information-theoretic quantities in the case of single-parameter metrology.

The single-parameter sensing paradigm can then be equivalently recast as a function approximation task, where the goal is to learn the target function:

$$f^*(u) = u. \quad (6)$$

It is important to note that the sensing loss function, $\mathcal{L}[f^*]$ in Eq. (2), depends on the number of shots S carried out to construct an estimate of the function. It notably depends on the prior probability distribution of the inputs $p(u)$. Therefore, let us choose the special case of single-shot estimation, i.e. $S = 1$, and suppose that the input distribution u obeys a zero-mean Gaussian distribution

$$p(u) = \frac{1}{\sqrt{2\pi}\sigma} e^{-\frac{u^2}{2\sigma^2}}. \quad (7)$$

Under these assumptions, the single-shot sensing loss of any given POVM $\{\hat{M}_j\}$ can be straightforwardly expanded by (see Ref. [48], see also Appendix A):

$$\mathcal{L}[f^*; S = 1] = \sigma^2 - \sigma^4 \mathcal{I}^{(1)}(0) - \sigma^6 \mathcal{I}^{(2)}(0) + \mathcal{O}(\sigma^8). \quad (8)$$

The second-order term corresponds to the Fisher information (FI) [30], and can be expressed as

$$\mathcal{I}^{(1)}(0) = \sum_{j=1}^K \frac{\left(x_j^{(1)}(0)\right)^2}{x_j(0)}, \quad (9)$$

where $x_j^{(n)}(0)$ denotes the n -th order derivative with respect to the unknown parameter u of the j -th measurement outcome evaluated at $u = 0$. The third-order term in the σ^2 expansion is associated with what is known as *Bhattacharyya information* [49]

$$\mathcal{I}^{(2)}(0) = \sum_{j=1}^K \left(\frac{x_j^{(1)}(0)x_j^{(3)}(0)}{x_j(0)} - \frac{(x_j^{(1)}(0))^2 x_j^{(2)}(0)}{2(x_j(0))^2} \right). \quad (10)$$

Consequently, the single-shot linear capacity can be viewed as a generating functional for a hierarchy of information measures: the Fisher information appears as the first-order contribution, followed by a series of higher-order Bhattacharyya-type terms.

These findings align with recent studies [47, 50] showing that the Fisher information provides a reliable precision bound only in the local regime, where the parameter is confined to a narrow neighborhood around a known reference value. When the parameter is distributed over a broad range, the FI alone becomes insufficient to characterize the fundamental limits of estimation. In such *global* scenarios, the higher-order Bhattacharyya information terms become essential, offering a more refined and accurate quantification of the system's estimation capabilities as they account for both the nonlinear response of the measurement outcomes and the intrinsically nonlocal character of estimation when the parameter varies over a wide range. Optimizing over all possible POVMs elevates these classical quantities to their quantum counterparts, giving rise to the quantum Fisher information and the quantum Bhattacharyya or Barankin-type bounds [51].

Consequently, the Capacity in Eq. (5) encapsulates all relevant information-theoretic contributions, both local and nonlocal, making it a natural figure of merit for sensing across all regimes. Its optimization not only recovers known bounds in the local limit but also may guide the design of improved measurement strategies in global scenarios and BQI-style tasks, where higher-order effects become essential.

C. Reservoir-based optimization

Optimizing the full sensing stack comprising the preparation of a metrologically useful state, the choice of POVM, and the classical post-processing used to compute the estimator presents substantial computational challenges. The parameter space is high dimensional, and the objective function $l[f^*]$ exhibits stochastic fluctuations under realistic conditions, particularly when the number of measurement shots S is small relative to the number of possible outcomes K . In this regime, gradient-based optimization methods often become unreliable or inefficient.

In this regime, a carefully designed optimization strategy is essential, since joint training of the sensing components otherwise becomes trapped in suboptimal regions of the landscape. To overcome this difficulty, we develop a tailored optimization scheme suited to the complex, nonconvex structure characteristic of supervised machine learning problems, including our sensing task.

Let us consider the supervised quantum machine learning scenario in which high-dimensional classical inputs \mathbf{u} are drawn from a fixed but unknown distribution $p(\mathbf{u})$. In practice, one has access to a finite training set consisting of N_{tr} independent and identically distributed (i.i.d.) samples, $\{\mathbf{u}^{(n)}\}_{n=1}^{N_{\text{tr}}}$, each paired with a corresponding label $f^*(\mathbf{u}^{(n)})$. These labels may be continuous, as in regression tasks (e.g., function fitting), or discrete, as in classification problems.

As discussed previously, the post-processing stage involves a linear combination of features, written as

$\mathbf{w}^T \mathbf{X}(\mathbf{u})$, where $\mathbf{w} \in \mathbb{R}^{K \times D}$ denotes the matrix of output weights and D is the dimensionality of the output space.

Therefore, we define the average loss over a dataset of N samples as

$$\hat{l}(\boldsymbol{\theta}, \mathbf{w}) = \frac{1}{N} \sum_{n=1}^N \left(f^*(\mathbf{u}^{(n)}) - f_{\text{est}}(\mathbf{u}^{(n)}) \right)^2, \quad (11)$$

as an estimator of Eq. ((2)). We note that in supervised learning, the loss function \mathcal{L} also depends on the target label $f^*(\mathbf{u}^{(n)})$ associated with each input $\mathbf{u}^{(n)}$, although for notational simplicity this dependence is not written explicitly in the arguments of \mathcal{L} throughout this article.

When the parameters $\boldsymbol{\theta}$ are randomly initialized but fixed, only the output weights \mathbf{w} are subject to optimization. This training paradigm is known as *reservoir computing* (RC), or equivalently, an *extreme learning machine* – a framework that has been widely studied in both classical and quantum contexts [22, 52–56]. One commonly used choice is the *linear regression* where the output is given by $\mathbf{w}^T \mathbf{z}$, and the loss is the standard mean-squared error, similarly to Eq. (2). In this case, the loss function $\hat{l}(\mathbf{w}, \mathbf{z})$ is convex in \mathbf{w} , allowing for efficient computation of a unique optimal solution $\mathbf{w}^*(\boldsymbol{\theta})$ that minimizes the loss.

If one wishes to optimize both the internal and the external parameters a straightforward approach would be to optimize both $\boldsymbol{\theta}$ and \mathbf{w} jointly by computing the gradients $\nabla_{\boldsymbol{\theta}} \hat{l}(\boldsymbol{\theta}, \mathbf{w})$ and $\nabla_{\mathbf{w}} \hat{l}(\boldsymbol{\theta}, \mathbf{w})$ and applying standard gradient descent. We show that it is advantageous to exploit the special structure of the problem, namely that the loss function \hat{l} is convex with respect to \mathbf{w} .

To this end, we introduce a method that carries out gradient-based optimization directly on the post-reservoir loss

$$\hat{\mathcal{L}}(\boldsymbol{\theta}) = \min_{\mathbf{w} \in \mathbb{R}^K} \hat{l}(\boldsymbol{\theta}, \mathbf{w}), \quad (12)$$

with the corresponding optimal weights $\mathbf{w}^*(\boldsymbol{\theta}) \equiv \arg \min_{\mathbf{w}} \hat{l}(\boldsymbol{\theta}, \mathbf{w})$. We can show that under reasonable assumptions, $\hat{\mathcal{L}}(\boldsymbol{\theta})$ can be approximated as a Gaussian random variable, $\hat{\mathcal{L}}(\boldsymbol{\theta}) \sim \mathcal{N}(\mu(\boldsymbol{\theta}), s(\boldsymbol{\theta}))$, see the detailed expression of $\mu(\boldsymbol{\theta}), s(\boldsymbol{\theta})$ in Appendix B.

We seek an optimization strategy that leverages both the bounded search domain and the regularity properties of the stochastic loss function $\hat{\mathcal{L}}(\boldsymbol{\theta})$. For this purpose, we adopt a tailored variant of the *Dividing RECTangles (DIRECT)* algorithm [57–60]. This method admits global convergence guarantees under adequate refinement and is further adapted to incorporate a physically motivated statistical metamodel of the loss landscape, thereby enhancing convergence efficiency and mitigating sensitivity to local minima.

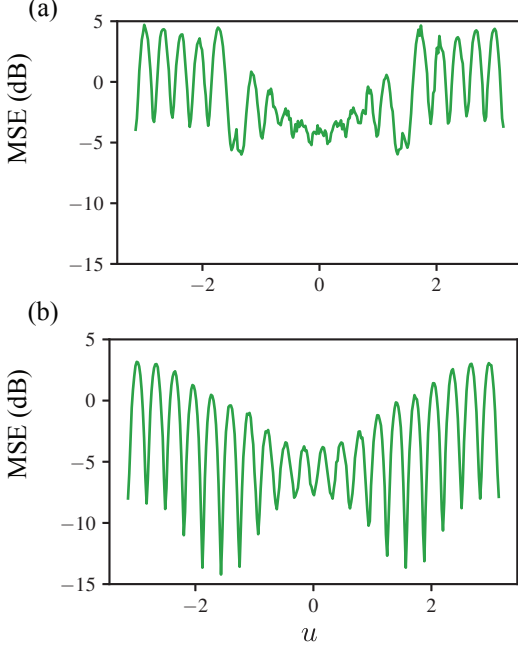


Figure 2. Results of the optimization for approximating the target function $f(u) = \sin(10u)$ where u is sampled from a Gaussian prior of width $\sigma = 0.7981$ and for a circuit with $n_{\text{en}} = 1$, $n_{\text{de}} = 0$, $L = 32$, and $S = 1$. (a) Mean squared error, $\text{MSE}(u)$, as a function of the true input phase u by indirect approximation of the target function, achieving $\mathbb{E}_u[\text{MSE}_1] \approx -2.9$ dB (b) Mean squared error, $\text{MSE}(u)$, as a function of the true input phase u by direct approximation of the target function achieving $\mathbb{E}_u[\text{MSE}_2] \approx -4.7$ dB (see Sec. II E of the main text).

D. Eigentasks analysis

Until now, our estimator has taken the form $f(\mathbf{u}) = \mathbf{w}^T \mathbf{X}(\mathbf{u})$, where $\mathbf{X}(\mathbf{u})$ denotes the empirical feature vector obtained from S measurement shots. This representation implicitly includes a linear combination of all possible measurement outcomes. However, in practice, certain features—or specific linear combinations of features—may contribute disproportionately to the overall noise relative to the information they provide. Retaining such noisy components can degrade performance and might lead to overfitting.

To mitigate this, one can identify and eliminate redundant or noise-dominated features, akin to the spirit of principal component analysis (PCA), which selects only the most informative directions in feature space. In our context, these optimal linear combinations of features are referred to as *eigentasks*, a concept first introduced in Ref. [3], and shown to minimize generalization error in supervised machine learning tasks with large-sized training datasets [61].

The key equation underlying the definition of eigen-

tasks is a generalized eigenvalue problem

$$\mathbf{V}\mathbf{r}^{(j)} = \beta_j^2 \mathbf{G}\mathbf{r}^{(j)}, \quad (13)$$

where $\mathbf{G} \equiv \mathbb{E}_{\mathbf{u}}[\mathbf{x}\mathbf{x}^T]$ and $\mathbf{V} \equiv \mathbb{E}_{\mathbf{u}}[\mathbf{\Sigma}]$ is the expected Gram and covariance matrix respectively. Each eigenvalue β_j^2 quantifies the MSE in constructing a system-specific function $y^{(j)}(\mathbf{u})$ given by

$$y^{(j)}(\mathbf{u}) = \sum_{j'} r_{j'}^{(j)} x_{j'}(\mathbf{u}). \quad (14)$$

The expected Capacity for the sensor sampled S times to estimate $y^{(j)}(\mathbf{u})$ is given by $1/(1 + \beta_j^2/S)$. In other words S/β_j^2 is the expected SNR of approximating that function with inputs sampled from the prior $p(\mathbf{u})$. The eigentasks and their associated SNRs are specific to the prior $p(\mathbf{u})$, the embedding and the remaining circuit parameters.

This formulation provides a systematic way to identify and rank linear combinations of features according to their information content since eigentasks with large SNR (i.e., small β_j^2/S) are more robust to sampling noise and therefore better suited for generalization. This observation suggests a dimensionality-reduction technique for supervised ML based on an estimator built from the first K_L eigentasks. A practical application of this feature-reduction technique to a specific ML problem implemented on a quantum processor suggested a cutoff K_L such that $\beta_{K_L}^2 \sim S$, later analytically confirmed in Ref. [61].

Consequently, the resulting estimator, based on the most informative eigentasks, takes the form

$$f(\mathbf{u}) = \sum_{j=1}^{K_L} w_{\text{et},j} y^{(j)}(\mathbf{u}), \quad (15)$$

where the weights $w_{\text{et},j}$ are trained on the reduced feature set. Finally, although the definition of eigentasks so far has assumed access to the idealized, infinite-shot features \mathbf{x} and an infinitely large training set, they can still be effectively approximated and remain practically useful under finite measurement shots and finite training dataset size [3].

E. Results

In this section we apply the general framework developed above in approximating arbitrary functions of a single parameter u which is drawn from a complex prior distribution. As already emphasized this is in stark contrast to more conventional Fisher information-based approaches which optimize accuracy only locally corresponding to $\sigma \rightarrow 0$ and are valid over a narrow dynamic range of the order $\sigma \sim 1/L$. Furthermore, following the sensing pipeline outlined in Sec. II B, we consider a training dataset consisting of $N_{\text{tr}} = 10000$ samples

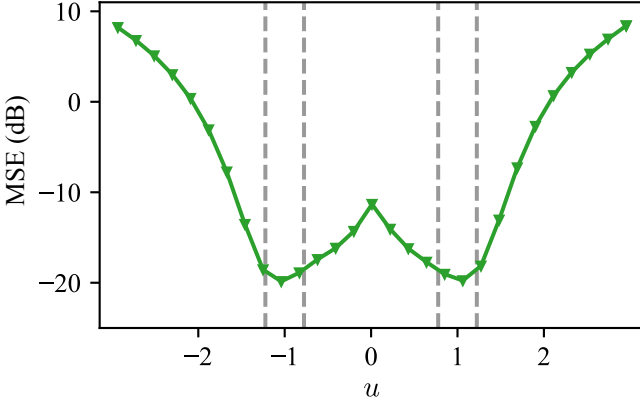


Figure 3. Results of the optimization for approximating the target function $f(u) = u$ where u is sampled from a symmetric mixture of Gaussian prior distributions of width $\sigma^2 = 0.05$ and for a circuit with $n_{\text{en}} = 1$, $n_{\text{de}} = 0$, $L = 32$, and $S = 1$. Mean squared error, $\text{MSE}(u)$, as a function of the true input phase u . The dashed grey lines correspond to the standard deviation around the respective means. The achieved precision is $\mathbb{E}_u[\text{MSE}] \approx -18.3$ dB compared to the optimal allowed $\mathbb{E}_u[\text{MSE}]_{\text{ult}} \approx -22.5$ dB.

independently drawn from the corresponding probability distribution. Finally, for all the results presented in this section we fix $S = 1$ i.e assuming single-shot experiments. While the choice $S = 1$ may initially appear restrictive, it is directly relevant to sensing scenarios where the signal varies between repetitions but is sampled from the same underlying distribution. Moreover, analyzing performance in the single-shot regime is critical for future applications involving large quantum many-body systems. In such systems, the exponentially large number of possible measurement outcomes, combined with a finite number of experimental repetitions, implies that most outcomes occur at most once, or not at all, thereby effectively exhibiting the characteristics of the single-shot sensing regime in practice.

Motivated by the successful application of a variational quantum algorithm in a trapped-ion platforms, and following Refs. [11, 13], we assume that the probe, entangler and decoder circuits take the form

$$U_{\text{em}}(u) = \mathcal{R}_z(u), \quad (16)$$

$$U_{\text{en}}(\boldsymbol{\theta}_{\text{en}}) = \mathcal{R}_x(\theta_{n_{\text{en}}}^{(3)}) \mathcal{T}_x(\theta_{n_{\text{en}}}^{(2)}) \mathcal{T}_z(\theta_{n_{\text{en}}}^{(1)}) \dots \mathcal{R}_x(\theta_1^{(3)}) \mathcal{T}_x(\theta_1^{(2)}) \mathcal{T}_z(\theta_1^{(1)}) \mathcal{R}_y\left(\frac{\pi}{2}\right), \quad (17)$$

$$U_{\text{de}}(\boldsymbol{\theta}_{\text{de}}) = \mathcal{R}_x\left(\frac{\pi}{2}\right) \mathcal{T}_z(\vartheta_1^{(1)}) \mathcal{T}_x(\vartheta_1^{(2)}) \mathcal{R}_x(\vartheta_1^{(3)}) \dots \mathcal{T}_z(\vartheta_{n_{\text{de}}}^{(1)}) \mathcal{T}_x(\vartheta_{n_{\text{de}}}^{(2)}) \mathcal{R}_x(\vartheta_{n_{\text{de}}}^{(3)}). \quad (18)$$

Here, n_{en} and n_{de} denote the number of layers in the entangler and decoder, respectively. The collective rotations and one-axis twisting operations are defined as $\mathcal{R}_\alpha(\phi) = e^{-\phi J_\alpha}$ and $\mathcal{T}_\alpha(\phi) = e^{-\phi J_\alpha^2}$, respectively, with $\alpha \in \{x, y, z\}$. The collective spin operators are given

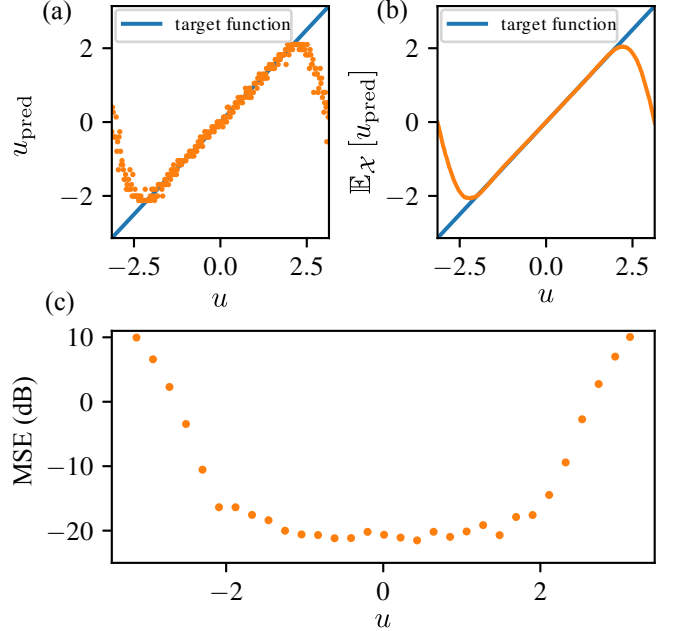


Figure 4. Results of the optimization for $n_{\text{en}} = 1$, $n_{\text{de}} = 2$, $\sigma = 0.7981$, $L = 32$, and $S = 1$. (a) Predicted output u_{pred} (orange dots) as a function of the input phase u for a single experimental repetition. The target function $f^*(u) = u$ is shown in blue. Each dot corresponds to a distinct measurement outcome, highlighting the stochasticity of the single-shot regime. (b) Averaged prediction $\langle u_{\text{pred}} \rangle$ over many repetitions, demonstrating convergence to the target function in a wide range around $u = 0$. (c) Mean squared error $\text{MSE}(u)$ as a function of the true phase u , quantifying the estimator's performance across the domain. Importantly, the achieved $\mathbb{E}_u[\text{MSE}] \approx -19.1$ dB is remarkably close to the ultimate bound of $\mathbb{E}_u[\text{MSE}]_{\text{ult}} \approx -20$ dB allowed by quantum mechanics.

by $J_\alpha \equiv \sum_{i=1}^L \hat{\sigma}_\alpha^{(i)}/2$, where $\hat{\sigma}_\alpha^{(i)}$ denotes the Pauli- α operator acting on the i -th qubit. We assume a projective measurement of the J_z observable, with eigenstates $|j; m\rangle$ satisfying $\mathbf{J}^2 |j; m\rangle = j(j+1) |j; m\rangle$ and $J_z |j; m\rangle = m |j; m\rangle$, where j and m correspond to the total angular momentum and its projection along the z -axis, respectively. Note that since our protocol employs global operations that conserve the total angular momentum, it is sufficient to restrict the analysis to the $j = L/2$ subspace, which is also the sector in which the maximum precision is attained. $X_k(u)$, the feature we measured, is the z -component of the total angular momentum. In practice, this z -component is measured by performing an ordinary computational basis measurement, and $X_k = k/L$ where k is the number of spin-up outcomes. Following the efficient optimization algorithm described in Sec. II C and further analyzed in Appendix D, we determine the optimal parameters $\boldsymbol{\theta}_{\text{en}}$, $\boldsymbol{\theta}_{\text{de}}$, and \mathbf{w} that minimize the loss function in Eq. (2).

Approximating a non-linear function—To illustrate the importance of our framework, we consider the task

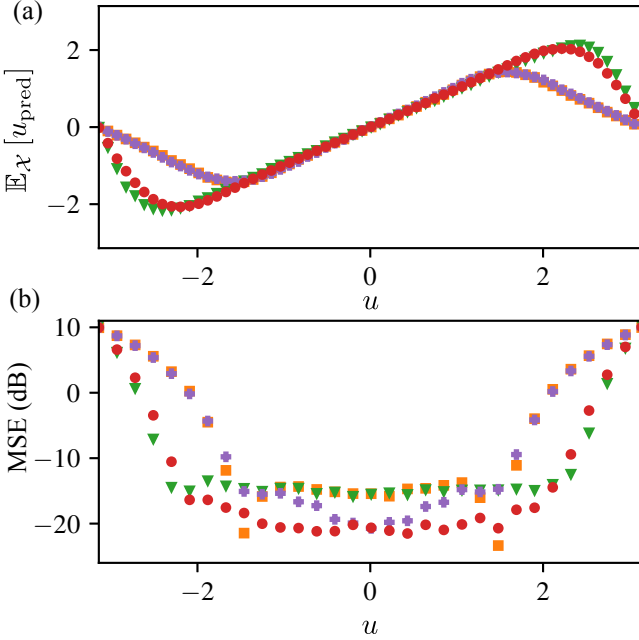


Figure 5. Results of the optimization for various circuit ansätze. Orange squares correspond to a circuit with depth $n_{\text{en}} = 0$ and $n_{\text{de}} = 0$, green triangles to $n_{\text{en}} = 1$ and $n_{\text{de}} = 0$, purple crosses to $n_{\text{en}} = 0$ and $n_{\text{de}} = 2$, and red dots to $n_{\text{en}} = 1$ and $n_{\text{de}} = 2$. (a) Average predicted output as a function of u for the different circuit depths. (b) Corresponding mean squared error for the same circuit configurations.

of approximating a non-trivial target function, $f(u) = \sin(10u)$, where the unknown parameter u is drawn from a Gaussian prior distribution

$$P_\sigma(u) = \frac{1}{\sqrt{2\pi}\sigma} \exp\left(-\frac{u^2}{2\sigma^2}\right), \quad (19)$$

while the domain is restricted to $u \in [-\pi, \pi]$ by rejecting samples outside this interval. We note that given the Gaussian form of the prior distribution, the training dataset size can be substantially reduced, if needed, by approximating the loss function using a Gauss–Hermite quadrature integration, as detailed in Appendix D.

As a first naive strategy, one could attempt to optimize the quantum circuit and the estimator to approximate the parameter u itself, by constructing a linear estimator of the form $u_{\text{est}} = \mathbf{w}^T \mathbf{X}(u)$. The target function is then approximated indirectly by applying f to the estimated parameter, i.e., $f(u_{\text{est}}) = \sin(10u_{\text{est}})$.

In contrast, within our approach, the entire sensing pipeline—including both the circuit and the estimator—is co-optimized directly for the task of approximating the target function $f(u) = \sin(10u)$, rather than the parameter u itself. Specifically, we seek to construct a linear estimator of the form $f_{\text{est}} = \mathbf{w}^T \mathbf{X}(u)$ that best approximates $f(u)$ by minimizing the cost function defined in Eq. (2).

This task-oriented optimization ensures that both the

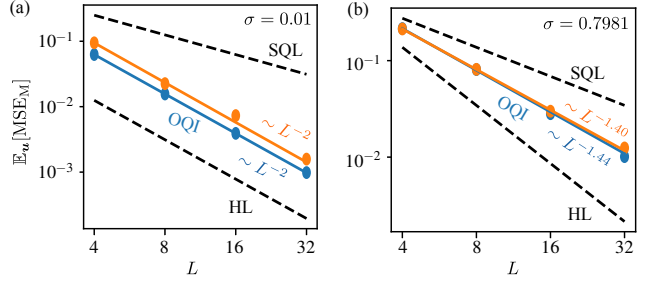


Figure 6. Scaling of the effective measurement variance $\mathbb{E}_u[\text{MSE}_M]$ as a function of the system size L for $n_{\text{en}} = 1$, $n_{\text{de}} = 2$ circuit and for (a) a narrow prior with $\sigma = 0.01$ and (b) a wide prior with $\sigma = 0.7981$. The blue solid line shows the scaling predicted by the optimal quantum interferometer (OQI), while the orange solid line shows the scaling achieved by our optimization algorithm. The upper and lower black dashed lines indicate the standard quantum limit (SQL) and the Heisenberg limit (HL), respectively.

feature extraction performed by the circuit and the final estimator are tailored to the inference objective. As a result, it can yield significantly improved performance—especially when the target function is highly nonlinear, such as $f(u) = \sin(10u)$. This improvement is clearly illustrated in Fig. 2, where we show the mean squared error $\text{MSE}(u) \equiv \mathbb{E}\left[(u - u_{\text{pred}})^2 | u\right]$, as function of the true value of the unknown phase for $\sigma = 0.7981$ and using a circuit with $n_{\text{en}} = 1$ and $n_{\text{de}} = 0$ layers.

To make the comparison even more concrete, in the naive two-step approach—where the circuit is first optimized to estimate u and the nonlinearity is applied afterward—we achieve an average error of $\mathbb{E}_u[\text{MSE}_1] \approx 0.51 \approx -2.9$ dB. In contrast, using our direct optimization strategy, the error is significantly reduced to $\mathbb{E}_u[\text{MSE}_2] \approx 0.34 \approx -4.7$ dB, highlighting the practical advantage of our task-specific co-optimization.

Function approximation for signals with a non-trivial prior—We next demonstrate our framework in the setting of estimating the single parameter u drawn from the non-trivial prior distribution

$$P(u) = \frac{c_1}{\sqrt{2\pi}\sigma_1} \exp\left(-\frac{(u - \mu_1)^2}{2\sigma_1^2}\right) + \quad (20)$$

$$\frac{c_2}{\sqrt{2\pi}\sigma_2} \exp\left(-\frac{(u - \mu_2)^2}{2\sigma_2^2}\right). \quad (21)$$

We choose $c_1 = c_2 = 1/2$, $\mu_1 = 1$, $\mu_2 = -1$ and $\sigma_1^2 = \sigma_2^2 = 0.05$. As illustrated in Fig. 3 where we employ a circuit with $n_{\text{en}} = 1$ and $n_{\text{de}} = 0$ layers, our approach achieves high estimation accuracy in regions near the peaks of the Gaussian components—i.e., within one standard deviation of each prior mean—while the performance naturally degrades in regions of low prior probability.

Benchmarking—Finally, and for benchmarking our framework with existing results in literature; see

Refs. [11, 13], we apply our framework in estimating a single parameter u drawn from the Gaussian prior of Eq. (19) with $\sigma = 0.7981$. Results of the optimization for $n_{\text{en}} = 1$, $n_{\text{de}} = 2$, $\sigma = 0.7981$, $L = 32$, and $S = 1$ are shown in Fig. 4. In particular, Fig. 4(a) illustrates the approximation of the target function $f^*(u) = u$ (shown in blue) based on a single experimental shot. Due to the stochastic nature of the measurement outcomes, different repetitions of the experiment yield different predictions. Averaging over many repetitions gives rise to the functional form shown in Fig. 4(b), which successfully captures the shape of the target function over a broad range around $u = 0$. The lower panel displays the mean squared error, $\text{MSE}(u)$, as a function of the true value of the unknown phase. Importantly, even for such shallow circuit, the achieved average error is $\mathbb{E}_u[\text{MSE}] \approx -19.1$ dB, which is very close to the ultimate limit of an optimal quantum interferometer (OQI) of $\mathbb{E}_u[\text{MSE}]_{\text{ult}} \approx -20$ dB as imposed by quantum mechanics [41].

We further investigate the performance of our algorithm using various circuit ansätze, as illustrated in Fig. 5, incorporating both tailored input states and effective POVMs. Our results are in complete agreement with those previously reported, thereby saturating the existing benchmarks in the literature and validating the effectiveness of our framework in reproducing state-of-the-art performance.

Going one step beyond we further study the scaling of an effective measurement variance $\mathbb{E}_u[\text{MSE}_M]$, where $1/\mathbb{E}_u[\text{MSE}_M] \equiv 1/\mathbb{E}_u[\text{MSE}] - 1/\sigma^2$ [11, 62], with respect to the system size L as illustrated in Fig. 6 for $n_{\text{en}} = 1$, $n_{\text{de}} = 2$ and for two representative values of σ . In both cases our optimization algorithm attains the scaling of an OQI and goes beyond the scaling of the standard quantum limit (SQL) while for sufficiently narrow priors it reaches the Heisenberg limit (HL), as expected.

1. Use of eigentasks

So far, the optimization of our sensing pipeline has relied on the full set of raw features obtained from the sensor to successfully approximate the target function. However, as discussed in Sec. IID, a promising alternative is to consider linear combinations of features—referred to as *eigentasks*—that exhibit a sufficiently high signal-to-noise ratio. Consequently, the optimization of the internal parameters of the entangling and decoding part of the circuit ansatz, as well as the estimator, must be revisited, since in principle the resulting optimal configurations generally depend on the number of eigentasks retained. Such modification arises from the cutoff criterion used to select eigentasks based on their signal-to-noise ratio, β_k^2 . In the special case where all eigentasks are preserved, the optimization reduce to the original setting, due to the linearity of both the feature transformation and the estimator.

Results in the special case of $n_{\text{en}} = 1$, $n_{\text{de}} = 2$,

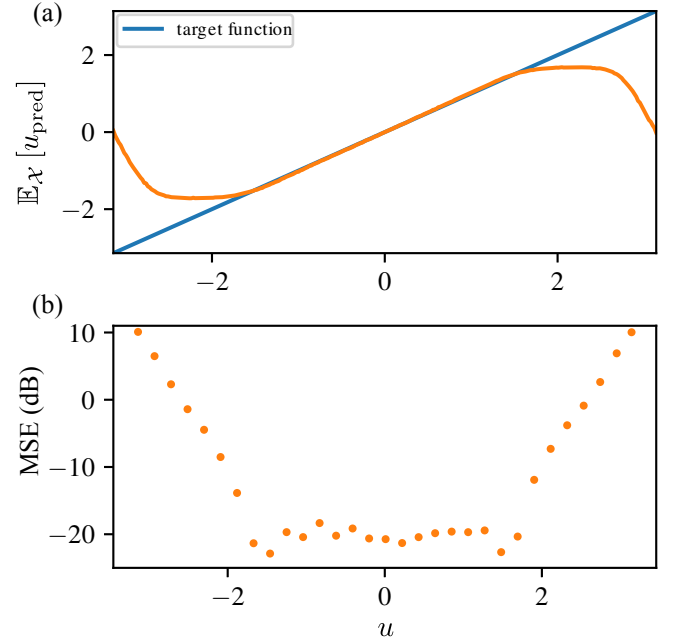


Figure 7. Results of the optimization for $n_{\text{en}} = 1$, $n_{\text{de}} = 2$, $\sigma = 0.7981$, $L = 32$, and $S = 1$ using the the first three non-trivial eigentasks with the highest SNR. (a) Averaged prediction $\langle u_{\text{pred}} \rangle$ over many repetitions, demonstrating convergence to the target function in a wide range around $u = 0$. (b) Mean squared error $\text{MSE}(u)$ as a function of the true phase u , quantifying the estimator's performance across the domain. The achieved $\mathbb{E}_u[\text{MSE}] \approx -17.1$ dB, although degraded, is remarkably close to the one with the use of all features illustrated in Fig. 4(c). This suggests that incorporating additional eigentasks can further enhance the estimation performance.

$L = 32$ and $S = 1$ are shown in Fig. 7, where the sensing pipeline has been optimized based on the three eigentasks with the highest SNR as defined in Eq. (13) and Eq. (14). We highlight that the eigentask coefficients defined in Eq. (13) are computed in the infinite-shot regime, but based on a finite training dataset of size $N_{\text{tr}} = 10000$. Surprisingly, we observe that the performance achieved using only a small number of eigentasks, although degraded, closely matches that of the full-feature case shown in Fig. 4, while the optimal parameters of the entangling and decoding circuits remain unchanged. Moreover, as shown in Fig. 8(a), the first non-trivial eigentask alone essentially reproduces the functional form of the target function, highlighting its dominant contribution.

III. DISCUSSION AND CONCLUSION

We have developed a data-driven supervised learning framework for quantum sensing in which state preparation, encoding, measurement, and classical estimation are optimized jointly with respect to a global infer-

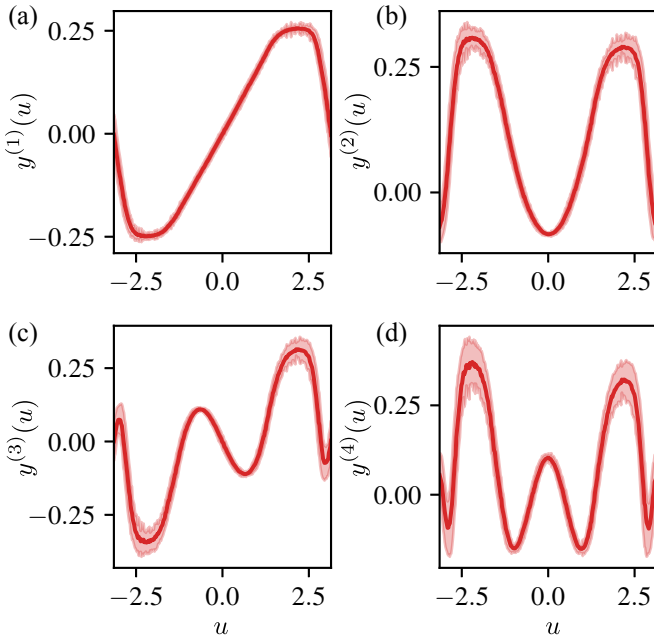


Figure 8. Functional form of the mean values (solid lines) and standard deviations (shaded regions) of the first four non-trivial eigentasks, shown in panels (a)-(d) respectively. These are obtained for the circuit ansatz and learning task described in Sec. II E 1. Notably, the first eigentask, panel (a), already reproduces the structure of the target function, $f(u) = u$, in a wide range around $u = 0$. As expected, the uncertainty in the mean values increases with the eigentask index (see main text).

ence task. Formulating quantum sensing in supervised-learning terms allows direct approximation of arbitrary nonlinear functions of stochastic inputs, extending the scope of quantum metrology beyond local Fisher-information bounds and connecting performance to a broader notion of functional capacity.

Technically, we introduced an efficient optimization procedure that integrates a reservoir-inspired estimator with post-reservoir loss minimization, enabling convergence to near-optimal solutions even in the single-shot

regime where sampling noise is strongest. The eigentask analysis further identifies noise-robust feature combinations that produce compact estimators while suppressing unstable or low-SNR modes.

Our results show that co-optimizing the entire sensing pipeline yields substantial gains over two-stage strategies in which parameter estimation precedes functional evaluation. The framework reproduces known benchmarks, accommodates general priors and nonlinear targets, and provides a unified approach for realistic sensing scenarios. These findings suggest a shift in quantum metrology toward integrated, data-driven codesign of sensors and inference algorithms.

Several directions follow from this work. A deeper theoretical link between functional capacity and quantum information bounds in multi-parameter and multi-shot settings would broaden the conceptual foundation. On the practical side, adapting the optimization framework to noisy intermediate-scale devices, incorporating hardware-aware ansätze, and benchmarking on experimental platforms such as trapped ions and superconducting circuits are natural next steps. Extending the current linear-estimator architecture to nonlinear or adaptive readouts may unlock further opportunities for quantum-enhanced sensing and learning.

IV. ACKNOWLEDGMENTS

We acknowledge Peter Zoller and Denis Vasilyev for fruitful discussions as well as Charles Fromont for critical reading and feedback on our manuscript. Research was sponsored by AFOSR MURI Grant No. FA9550-22-1-0203 and by the Army Research Office under Grant No. W911NF-25-1-0261. The views and conclusions contained in this document are those of the authors and should not be interpreted as representing the official policies, either expressed or implied, of the Army Research Office or the U.S. Government. The U.S. Government is authorized to reproduce and distribute reprints for Government purposes notwithstanding any copyright notation herein.

- [1] M. Schuld and N. Killoran, Is quantum advantage the right goal for quantum machine learning?, *PRX Quantum* **3**, 030101 (2022).
- [2] J. Liu, F. Wilde, A. A. Mele, X. Jin, L. Jiang, and J. Eisert, Stochastic noise can be helpful for variational quantum algorithms, *Phys. Rev. A* **111**, 052441 (2025).
- [3] F. Hu, G. Angelatos, S. A. Khan, M. Vives, E. Türeci, L. Bello, G. E. Rowlands, G. J. Ribeill, and H. E. Türeci, Tackling sampling noise in physical systems for machine learning applications: Fundamental limits and eigentasks, *Phys. Rev. X* **13**, 041020 (2023).
- [4] F. Hu, S. A. Khan, N. T. Bronn, G. Angelatos, G. E. Rowlands, G. J. Ribeill, and H. E. Türeci, Overcoming the coherence time barrier in quantum machine learning on temporal data, *Nature Communications* **15**, 7491 (2024).
- [5] V. Giovannetti, S. Lloyd, and L. Maccone, Quantum-enhanced measurements: Beating the standard quantum limit, *Science* **306**, 1330 (2004).
- [6] V. Giovannetti, S. Lloyd, and L. Maccone, Quantum metrology, *Phys. Rev. Lett.* **96**, 010401 (2006).
- [7] D. Braun, G. Adesso, F. Benatti, R. Floreanini, U. Marzolino, M. W. Mitchell, and S. Pirandola, Quantum-

enhanced measurements without entanglement, *Rev. Mod. Phys.* **90**, 035006 (2018).

[8] E. Davis, G. Bentsen, and M. Schleier-Smith, Approaching the heisenberg limit without single-particle detection, *Phys. Rev. Lett.* **116**, 053601 (2016).

[9] M. Koppenhöfer, P. Groszkowski, and A. A. Clerk, Squeezed superradiance enables robust entanglement-enhanced metrology even with highly imperfect readout, *Phys. Rev. Lett.* **131**, 060802 (2023).

[10] Z. Li, S. Colombo, C. Shu, G. Velez, S. Pilatowsky-Cameo, R. Schmied, S. Choi, M. Lukin, E. Pedrozo-Peña, and V. Vuletić, Improving metrology with quantum scrambling, *Science* **380**, 1381 (2023), <https://www.science.org/doi/pdf/10.1126/science.adg9500>.

[11] R. Kaubruegger, D. V. Vasilyev, M. Schulte, K. Hammerer, and P. Zoller, Quantum variational optimization of ramsey interferometry and atomic clocks, *Phys. Rev. X* **11**, 041045 (2021).

[12] R. Kaubruegger, A. Shankar, D. V. Vasilyev, and P. Zoller, Optimal and variational multiparameter quantum metrology and vector-field sensing, *PRX Quantum* **4**, 020333 (2023).

[13] C. D. Marciak, T. Feldker, I. Pogorelov, R. Kaubruegger, D. V. Vasilyev, R. van Bijnen, P. Schindler, P. Zoller, R. Blatt, and T. Monz, Optimal metrology with programmable quantum sensors, *Nature* **603**, 604 (2022).

[14] J. R. McClean, S. Boixo, V. N. Smelyanskiy, R. Babbush, and H. Neven, Barren plateaus in quantum neural network training landscapes, *Nature Communications* **9**, 4812 (2018).

[15] M. Schuld, R. Sveke, and J. J. Meyer, Effect of data encoding on the expressive power of variational quantum-machine-learning models, *Physical Review A* **103**, 032430 (2021).

[16] Y. Wu, J. Yao, P. Zhang, and H. Zhai, Expressivity of quantum neural networks, *Physical Review Research* **3**, L032049 (2021).

[17] Y. Du, Z. Tu, X. Yuan, and D. Tao, Efficient Measure for the Expressivity of Variational Quantum Algorithms, *Physical Review Letters* **128**, 080506 (2022), publisher: American Physical Society.

[18] A. W. Harrow and R. A. Low, Random quantum circuits are approximate 2-designs, *Communications in Mathematical Physics* **291**, 257 (2009).

[19] J. Dambre, D. Verstraeten, B. Schrauwen, and S. Massar, Information Processing Capacity of Dynamical Systems, *Scientific Reports* **2**, 514 (2012).

[20] K. Fujii and K. Nakajima, Harnessing Disordered-Ensemble Quantum Dynamics for Machine Learning, *Physical Review Applied* **8**, 024030 (2017).

[21] J. Chen, H. I. Nurdin, and N. Yamamoto, Temporal Information Processing on Noisy Quantum Computers, *Physical Review Applied* **14**, 024065 (2020).

[22] L. G. Wright and P. L. McMahon, The Capacity of Quantum Neural Networks, [arXiv:1908.01364 \[quant-ph\]](https://arxiv.org/abs/1908.01364) (2019).

[23] J. García-Beni, G. L. Giorgi, M. C. Soriano, and R. Zambrini, Scalable photonic platform for real-time quantum reservoir computing, *Physical Review Applied* **20**, 014051 (2023).

[24] W. D. Kalfus, G. J. Ribeill, G. E. Rowlands, H. K. Krovi, T. A. Ohki, and L. C. G. Govia, Hilbert space as a computational resource in reservoir computing, *Physical Review Research* **4**, 033007 (2022).

[25] M. Kornjača, H.-Y. Hu, C. Zhao, J. Wurtz, P. Weinberg, M. Hamdan, A. Zhdanov, S. H. Cantu, H. Zhou, R. A. Bravo, K. Bagnall, J. I. Basham, J. Campo, A. Choukri, R. DeAngelo, P. Frederick, D. Haines, J. Hammett, N. Hsu, M.-G. Hu, F. Huber, P. N. Jepsen, N. Jia, T. Karolyshyn, M. Kwon, J. Long, J. Lopatin, A. Lukin, T. Macri, O. Marković, L. A. Martínez-Martínez, X. Meng, E. Ostroumov, D. Paquette, J. Robinson, P. S. Rodriguez, A. Singh, N. Sinha, H. Thoreen, N. Wan, D. Waxman-Lenz, T. Wong, K.-H. Wu, P. L. S. Lopes, Y. Boger, N. Gemelke, T. Kitagawa, A. Keesling, X. Gao, A. Bylinskii, S. F. Yelin, F. Liu, and S.-T. Wang, Large-scale quantum reservoir learning with an analog quantum computer, [arXiv:2407.02553 \[quant-ph\]](https://arxiv.org/abs/2407.02553) (2024).

[26] S.-Q. Gong, M.-C. Chen, H.-L. Liu, H. Su, Y.-C. Gu, H.-Y. Tang, M.-H. Jia, Y.-H. Deng, Q. Wei, H. Wang, H.-S. Zhong, X. Jiang, L. Li, N.-L. Liu, C.-Y. Lu, and J.-W. Pan, Enhanced image recognition using gaussian boson sampling, [arXiv:2506.19707 \[quant-ph\]](https://arxiv.org/abs/2506.19707) (2025).

[27] V. Cimini, M. M. Sohoni, F. Presutti, B. K. Malia, S.-Y. Ma, R. Yanagimoto, T. Wang, T. Onodera, L. G. Wright, and P. L. McMahon, Large-scale quantum reservoir computing using a gaussian boson sampler, [arXiv:2505.13695 \[quant-ph\]](https://arxiv.org/abs/2505.13695) (2025).

[28] V. Havlíček, A. D. Cárcoles, K. Temme, A. W. Harrow, A. Kandala, J. M. Chow, and J. M. Gambetta, Supervised learning with quantum-enhanced feature spaces, *Nature* **567**, 209 (2019).

[29] Y. Shen, N. C. Harris, S. Skirlo, M. Prabhu, T. Baehr-Jones, M. Hochberg, X. Sun, S. Zhao, H. Larochelle, D. Englund, and M. Soljačić, Deep learning with coherent nanophotonic circuits, *Nature Photonics* **11**, 441 (2017).

[30] S. M. Kay, *Fundamentals of Statistical Signal Processing: Estimation Theory* (Prentice Hall, 1997).

[31] C. W. Helstrom, Quantum detection and estimation theory, *Journal of Statistical Physics* **1**, 231 (1969).

[32] S. L. Braunstein and C. M. Caves, Statistical distance and the geometry of quantum states, *Phys. Rev. Lett.* **72**, 3439 (1994).

[33] R. Kaubruegger, P. Silvi, C. Kokail, R. van Bijnen, A. M. Rey, J. Ye, A. M. Kaufman, and P. Zoller, Variational spin-squeezing algorithms on programmable quantum sensors, *Phys. Rev. Lett.* **123**, 260505 (2019).

[34] E. Pedrozo-Peña, S. Colombo, C. Shu, A. F. Adiyatullin, Z. Li, E. Mendez, B. Braverman, A. Kawasaki, D. Akamatsu, Y. Xiao, and V. Vuletić, Entanglement on an optical atomic-clock transition, *Nature* **588**, 414 (2020).

[35] S. Colombo, E. Pedrozo-Peña, A. F. Adiyatullin, Z. Li, E. Mendez, C. Shu, and V. Vuletić, Time-reversal-based quantum metrology with many-body entangled states, *Nature Physics* **18**, 925 (2022).

[36] B. Koczor, S. Endo, T. Jones, Y. Matsuzaki, and S. C. Benjamin, Variational-state quantum metrology, *New Journal of Physics* **22**, 083038 (2020).

[37] J. J. Meyer, J. Borregaard, and J. Eisert, A variational toolbox for quantum multi-parameter estimation, *npj Quantum Information* **7**, 89 (2021).

[38] J. Yang, S. Pang, Z. Chen, A. N. Jordan, and A. del Campo, Variational principle for optimal quantum controls in quantum metrology, *Phys. Rev. Lett.* **128**, 160505 (2022).

[39] B. MacLellan, P. Roztocki, S. Czischek, and R. G. Melko, End-to-end variational quantum sensing, *npj Quantum Information* **10**, 118 (2024).

[40] T. Ilias, Biasing quantum trajectories for enhanced sensing, *Phys. Rev. A* **111**, 042432 (2025).

[41] K. Macieszczak, M. Fraas, and R. Demkowicz-Dobrzański, Bayesian quantum frequency estimation in presence of collective dephasing, *New Journal of Physics* **16**, 113002 (2014).

[42] R. R. Allen, F. Machado, I. L. Chuang, H.-Y. Huang, and S. Choi, *Quantum computing enhanced sensing* (2025), arXiv:2501.07625 [quant-ph].

[43] S. A. Khan, S. Prabhu, L. G. Wright, and P. L. McMahon, *Quantum computational-sensing advantage* (2025), arXiv:2507.16918 [quant-ph].

[44] M. G. Paris, Quantum estimation for quantum technology, *International Journal of Quantum Information* **07**, 125 (2008).

[45] M. Jarzyna and R. Demkowicz-Dobrzański, True precision limits in quantum metrology, *New Journal of Physics* **17**, 013010 (2015).

[46] W. Górecki, R. Demkowicz-Dobrzański, H. M. Wiseman, and D. W. Berry, π -corrected heisenberg limit, *Phys. Rev. Lett.* **124**, 030501 (2020).

[47] D. V. Vasilyev, A. Shankar, R. Kaubruegger, and P. Zoller, *Optimal multiparameter metrology: The quantum compass solution* (2024), arXiv:2404.14194 [quant-ph].

[48] F. Hu, *Quantum Machine Learning in Noisy Intermediate-Scale Quantum Era*, Phd thesis, Princeton University (2025).

[49] A. Bhattacharyya, On some analogues of the amount of information and their use in statistical estimation (contd.), *Sankhyā: The Indian Journal of Statistics (1933-1960)* **8**, 201 (1947).

[50] Y. Li, L. Pezzè, M. Gessner, Z. Ren, W. Li, and A. Smerzi, Frequentist and bayesian quantum phase estimation, *Entropy* **20**, 10.3390/e20090628 (2018).

[51] M. Gessner and A. Smerzi, Hierarchies of frequentist bounds for quantum metrology: From cramér-rao to barankin, *Phys. Rev. Lett.* **130**, 260801 (2023).

[52] G.-B. Huang, Q.-Y. Zhu, and C.-K. Siew, Extreme learning machine: a new learning scheme of feedforward neural networks, in *2004 IEEE International Joint Conference on Neural Networks (IEEE Cat. No.04CH37541)* (IEEE, 2004).

[53] S. Ortín, M. C. Soriano, L. Pesquera, D. Brunner, D. San-Martín, I. Fischer, C. R. Mirasso, and J. M. Gutiérrez, A Unified Framework for Reservoir Computing and Extreme Learning Machines based on a Single Time-delayed Neuron, *Scientific Reports* **5**, 14945 (2015).

[54] P. Mujal, R. Martínez-Peña, J. Nokkala, J. García-Beni, G. L. Giorgi, M. C. Soriano, and R. Zambrini, Opportunities in Quantum Reservoir Computing and Extreme Learning Machines, *Advanced Quantum Technologies* **4**, 2100027 (2021).

[55] C. M. Wilson, J. S. Otterbach, N. Tezak, R. S. Smith, A. M. Polloreno, P. J. Karalekas, S. Heidel, M. S. Alam, G. E. Crooks, and M. P. da Silva, Quantum Kitchen Sinks: An algorithm for machine learning on near-term quantum computers, arXiv:1806.08321 [quant-ph] (2019).

[56] L. Innocenti, S. Lorenzo, I. Palmisano, A. Ferraro, M. Paternostro, and G. M. Palma, On the potential and limitations of quantum extreme learning machines, *Communications Physics* **6**, 118 (2023).

[57] D. R. Jones, C. D. Perttunen, and B. E. Stuckman, Lipschitzian optimization without the lipschitz constant, *Journal of Optimization Theory and Applications* **79**, 157 (1993).

[58] H. Liu, S. Xu, X. Wang, J. Wu, and Y. Song, A global optimization algorithm for simulation-based problems via the extended direct scheme, *Engineering optimization* **47** (2014).

[59] P. Nicholas, A dividing rectangles algorithm for stochastic simulation optimization, in *Proceedings of the 14th INFORMS Computing Society Conference* (Richmond, Virginia, 2015) pp. 47–61.

[60] D. Finkel and C. Kelley, Convergence analysis of the direct algorithm, *N. C. State Univ.* **14** (2004).

[61] F. Hu and X. Gao, Generalization error in quantum machine learning in the presence of sampling noise, arXiv:2410.14654 [quant-ph] (2024).

[62] T. G. Thurtell and A. Miyake, Optimizing one-axis twists for variational bayesian quantum metrology, *Phys. Rev. Res.* **6**, 023179 (2024).

[63] K. Mitarai, M. Negoro, M. Kitagawa, and K. Fujii, Quantum circuit learning, *Phys. Rev. A* **98**, 032309 (2018).

[64] M. Schuld, V. Bergholm, C. Gogolin, J. Izaac, and N. Killoran, Evaluating analytic gradients on quantum hardware, *Phys. Rev. A* **99**, 032331 (2019).

Appendix A: Sensing Loss, Fisher Information and Bhattacharyya Information

In this section we establish an explicit relation between the functional $L[f; S]$ and *Fisher information* $\mathcal{I}(u)$. To this end, we emphasize that $L[f; S]$ depends non-trivially on the sample size S but is independent of the parameter u , whereas $\mathcal{I}(u)$ depends on u and it exhibits a trivial linear scaling for S independent shots. It is thus reasonable to fix the value of S and u with the natural choice being

$$S = 1, \quad \text{and} \quad u = 0. \quad (\text{A1})$$

Let us then suppose that the input u obeys a *zero-mean* Gaussian distribution:

$$p(u) = \frac{1}{\sqrt{2\pi}\sigma} e^{-\frac{u^2}{2\sigma^2}}. \quad (\text{A2})$$

An important lemma in probability theory is the Gaussian *integration by parts* formula: for any function $F(u)$

$$\int_{-\infty}^{\infty} F'(u) \frac{1}{\sqrt{2\pi}\sigma} e^{-\frac{u^2}{2\sigma^2}} du = - \int_{-\infty}^{\infty} F(u) \frac{d}{du} \left(\frac{1}{\sqrt{2\pi}\sigma} e^{-\frac{u^2}{2\sigma^2}} \right) du. \quad (\text{A3})$$

Namely,

$$\mathbb{E}_u[F'(u)] = \frac{1}{\sigma^2} \mathbb{E}_u[uF(u)]. \quad (\text{A4})$$

By plugging the functions $x_j(u) = \text{Tr}\{\hat{\rho}(u)\hat{M}_j\}$ into $F(u)$, we get [3]

$$\begin{aligned} L[f = u; S = 1] &= \mathbb{E}_u[f(u)^2] - \mathbb{E}_u[f(u)\mathbf{x}(u)]^T \left(\mathbf{G} + \frac{1}{S} \mathbf{V} \right)^{-1} \mathbb{E}_u[f(u)\mathbf{x}(u)] = \sigma^2 - \mathbb{E}_u[u\mathbf{x}(u)]^T \mathbf{D}^{-1} \mathbb{E}_u[u\mathbf{x}(u)] \\ &= \sigma^2 - \sum_{j=1}^K \mathbf{D}_{jj}^{-1} \cdot \mathbb{E}_u[u x_j(u)]^2 = \sigma^2 - \sum_{j=1}^K \frac{1}{\mathbb{E}_u[x_j(u)]} \cdot \left(\sigma^2 \mathbb{E}_u \left[\frac{dx_j}{du}(u) \right] \right)^2 \\ &= \sigma^2 - \sigma^4 \sum_{j=1}^K \frac{1}{\mathbb{E}_u[x_j(u)]} \left(\mathbb{E}_u \left[\frac{dx_j}{du}(u) \right] \right)^2, \end{aligned} \quad (\text{A5})$$

where $\mathbf{G} \equiv \mathbb{E}_u[\mathbf{x}\mathbf{x}^T]$, $\mathbf{V} \equiv \mathbb{E}_u[\Sigma]$ and $\mathbf{D}_{j,j'} = \delta_{j,j'} \mathbb{E}_u[x_j]$. Therefore,

$$\lim_{\sigma^2 \rightarrow 0} \frac{1}{\sigma^2} \left(1 - \frac{1}{\sigma^2} L[f = u; S = 1] \right) = \sum_{j=1}^K \frac{1}{x_j(0)} \left(\frac{dx_j}{du}(0) \right)^2 = \mathcal{I}(0). \quad (\text{A6})$$

In general, letting $u = \sigma v$ we have

$$\mathbb{E}_u[F(u)] = \mathbb{E}_u \left[F(0) + \sigma v F'(0) + \frac{1}{2} \sigma^2 v^2 F''(0) + \dots \right] = F(0) + \frac{\sigma^2}{2} F''(0) + O(\sigma^4). \quad (\text{A7})$$

Therefore, from Eq. (A5) we can express $C[f = u; S = 1]$ as

$$L[f = u; S = 1] = \sigma^2 - \sigma^4 \sum_{j=1}^K \frac{1}{x_j(0) + \frac{\sigma^2}{2} x_j''(0) + O(\sigma^4)} \left(x_j'(0) + \frac{\sigma^2}{2} x_j'''(0) + O(\sigma^4) \right)^2 \quad (\text{A8})$$

$$= \sigma^2 - \sigma^4 \underbrace{\sum_{j=1}^K \frac{x_j'(0)^2}{x_j(0)}}_{\text{Fisher Information}} - \sigma^6 \underbrace{\sum_{j=1}^K \left(\frac{x_j'(0)x_j'''(0)}{x_j(0)} - \frac{x_j'(0)^2 x_j''(0)}{2x_j^2(0)} \right)}_{\text{Bhattacharyya Information}} + O(\sigma^8), \quad (\text{A9})$$

where higher order terms in σ^2 -expansion give rise to *Bhattacharyya Information*.

In other words, the *single-shot sensing loss* serves as a generating functional for the Fisher information and, more generally, for the entire hierarchy of Bhattacharyya informations. The Fisher information quantifies the attainable accuracy of parameter estimation in the regime where the unknown parameter is restricted to a sufficiently local region.

However, when the parameter is distributed more broadly, the Fisher information alone no longer provides a complete characterization of the fundamental estimation limits. In this regime, higher-order Bhattacharyya information becomes essential, as it offers a refined description of the ultimate precision bounds of the metrological system [47].

There is a simple way to compare the derivation above and the Bhattacharyya bounds derivation in Ref. [47]. Supposing a quadratic loss for outcome j , we have

$$L = \sum_{j=1}^K \int (u - v_j)^2 x_j(u) p(u) du, \quad (\text{A10})$$

where v_j can be regarded as a single-shot estimator when obtaining the outcome j . The optimal $\{v_j\}$ is obtained by solving

$$\frac{\partial L}{\partial v_j} = -2 \int (u - v_j^*) x_j(u) p(u) du = 0, \quad (\text{A11})$$

whose solution is

$$v_j^* = \frac{\int u x_j(u) p(u) du}{\int x_j(u) p(u) du} = \frac{\mathbb{E}_u[ux_j]}{\mathbb{E}_u[x_j]}. \quad (\text{A12})$$

This is exactly the Eq.(C12) in Ref. [3], when taking $S = 1$ and $f(u) = u$; it is also the Eq.(14) in Ref. [47].

Appendix B: Cumulant Analysis of Function of Features with Quantum Shot Noise

In this section, we show an important result to characterize the behavior of any function of features with quantum shot noise. In Appendix C, we will use this result to prove that the post-reservoir loss in Eq. (12) is approximately Gaussian.

We recall in Sec. II B we define the noisy features as the empirical means of finite shots

$$\mathbf{X} = \frac{1}{S} \sum_s \mathbf{X}^{(s)} = \mathbf{x} + \boldsymbol{\zeta}, \quad (\text{B1})$$

where all single-shot features $\mathbf{X}^{(s)}$ are i.i.d. sampled from physical systems. Here, we absorb the scaling factor $1/\sqrt{S}$ into the shot noise term $\boldsymbol{\zeta}$. According to the homogeneity of cumulants, we can let the j -th order cumulant of $\boldsymbol{\zeta}$ be $\kappa_j[\boldsymbol{\zeta}] = \frac{1}{S^{j-1}} \boldsymbol{\kappa}^{(j)}$ where and $\boldsymbol{\kappa}^{(j)}$ must be an S -independent order- j tensor. For example, $\kappa_1[\boldsymbol{\zeta}] = \mathbb{E}[\boldsymbol{\zeta}] = \mathbf{0}$ and $\kappa_2[\boldsymbol{\zeta}] = \text{Cov}[\boldsymbol{\zeta}] = \frac{1}{S} \boldsymbol{\Sigma}$. Particularly for quantum sampling noise, we have $\boldsymbol{\kappa}^{(2)} = \boldsymbol{\Sigma} = \text{diag}(\mathbf{x}) - \mathbf{x}\mathbf{x}^T$. In this section, we focus on the expectation over shot noise, conditioned on a fixed input \mathbf{u} . Therefore, we use $\mathbb{E}[g]$ and $\text{Cov}[g]$ to abbreviate $\mathbb{E}[g|\mathbf{u}]$ and $\text{Cov}[g|\mathbf{u}]$ for arbitrary g .

In this appendix, we are going to analyze the cumulants of a function of the noisy features $\mathbf{X}(\mathbf{u})$, and prove that $\mathcal{F}(\mathbf{X})$ can be approximated by

$$\mathcal{F}(\mathbf{X}) \approx \mathcal{N} \left(\mathcal{F}(\mathbf{x}) + \frac{1}{2S} \sum_{j,j'} \frac{\partial^2 \mathcal{F}(\mathbf{x})}{\partial z_k \partial z_{j'}} \Sigma_{jj'}, \frac{1}{S} \sum_{j,j'} \left(\frac{\partial \mathcal{F}(\mathbf{x})}{\partial z_j} \frac{\partial \mathcal{F}(\mathbf{x})}{\partial z_{j'}} \right) \Sigma_{jj'} \right). \quad (\text{B2})$$

More precisely, when performing a $\frac{1}{S}$ -expansion of all cumulants of $\mathcal{F}(\mathbf{X})$ and retaining only terms up to order $\frac{1}{S}$, we find that the expectation $\kappa_1(\mathcal{F}(\mathbf{X})) = \mathbb{E}[\mathcal{F}(\mathbf{X})]$ and the covariance $\kappa_2(\mathcal{F}(\mathbf{X})) = \text{Cov}[\mathcal{F}(\mathbf{X})]$ both have non-vanishing contributions at order $\frac{1}{S}$ (see Appendix B 2). In contrast, for all $M \geq 3$ the higher-order cumulants $\kappa_M(\mathcal{F}(\mathbf{X}))$ vanish faster, namely $\kappa_M(\mathcal{F}(\mathbf{X})) = o(\frac{1}{S})$ (see Appendix B 3).

1. $(1/S)$ -expansion of function of noisy features

Before analyzing the cumulants of $\mathcal{F}(\mathbf{X})$, we first present an important result which will be repeatedly used in later computations. That is, for any function $\mathcal{G}(\mathbf{z})$, we show that $\mathcal{G}(\mathbf{X}) = \mathcal{G}(\mathbf{x} + \boldsymbol{\zeta})$ has expectation with $\frac{1}{S}$ -expansion:

$$\mathbb{E}[\mathcal{G}(\mathbf{X})] = \mathcal{G}(\mathbf{x}) + \frac{1}{2S} \sum_{j,j'} \frac{\partial^2 \mathcal{G}(\mathbf{x})}{\partial z_j \partial z_{j'}} \Sigma_{jj'} + o\left(\frac{1}{S}\right). \quad (\text{B3})$$

Such expression can be straightforwardly proven by writing down the Taylor expansion of $\mathcal{G}(\mathbf{X})$

$$\begin{aligned}\mathbb{E}[\mathcal{G}(\mathbf{X})] &= \mathbb{E}[\mathcal{G}(x_1 + \zeta_1, \dots, x_K + \zeta_K)] \\ &= \mathbb{E}[\mathcal{G}(\mathbf{x})] + \sum_{m=1}^{\infty} \sum_{j_1, \dots, j_m} \frac{1}{m!} \mathbb{E}[\partial_{j_1} \cdots \partial_{j_m} \mathcal{G}(\mathbf{x}) \zeta_{j_1} \cdots \zeta_{j_m}] \\ &= \mathcal{G}(\mathbf{x}) + \sum_{m=1}^{\infty} \sum_{j_1, \dots, j_m} \frac{1}{m!} \partial_{j_1} \cdots \partial_{j_m} \mathcal{G}(\mathbf{x}) \mathbb{E}[\zeta_{j_1} \cdots \zeta_{j_m}],\end{aligned}\tag{B4}$$

where $\mathbb{E}[\zeta_{j_1} \cdots \zeta_{j_m}]$ are the central moments of \mathbf{X} , which can be expressed in terms of cumulants of ζ :

$$\begin{aligned}\mathbb{E}[\mathcal{G}(\mathbf{X})] &= \mathcal{G}(\mathbf{x}) + \sum_{m=1}^{\infty} \sum_{j_1, \dots, j_m} \frac{1}{m!} \partial_{j_1} \cdots \partial_{j_m} \mathcal{G}(\mathbf{x}) \sum_{\pi \text{ of } [m] \text{ with no single set } B \in \pi, |B| \geq 2} \prod_{i \in B} \kappa_{|B|}(\zeta_{j_i} : i \in B) \\ &= \mathcal{G}(\mathbf{x}) + \sum_{m=1}^{\infty} \sum_{j_1, \dots, j_m} \frac{1}{m!} \partial_{j_1} \cdots \partial_{j_m} \mathcal{G}(\mathbf{x}) \sum_{\pi \text{ of } [m] \text{ with no single set}} \left(\frac{1}{S}\right)^{m-|\pi|} \prod_{B \in \pi, |B| \geq 2} \kappa_{j_{B_1} \cdots j_{B_{|B|}}}.\end{aligned}\tag{B5}$$

$\kappa_{|B|}(\zeta_{j_i} : i \in B)$ represents the components $|B|$ -th order tensor $\kappa^{(|B|)} / S^{|B|-1}$, whose indices are $\{j_i\}_{i \in B}$. We also emphasize here that $m - |\pi| \geq \lceil \frac{m}{2} \rceil$, since all $|B| = 1$ contributes nothing (first order cumulant always vanishes $\kappa_1(\zeta_j) \equiv 0$) in summation and thus they are excluded. Then by taking the truncation at $m = 2$, we can obtain Eq. (B3) directly.

2. First and second order cumulant

Now we can perform the cumulant analysis of $\mathcal{F}(\mathbf{X})$. For the first order cumulant (expectation), we just simply set $\mathcal{G} = \mathcal{F}$ in Eq. (B3):

$$\mathbb{E}[\mathcal{F}(\mathbf{X})] = \mathcal{F}(\mathbf{x}) + \frac{1}{2S} \sum_{j,j'} \frac{\partial^2 \mathcal{F}(\mathbf{x})}{\partial z_j \partial z_{j'}} \boldsymbol{\Sigma}_{jj'} + o\left(\frac{1}{S}\right).\tag{B6}$$

Similarly, the second order moment of $\mathcal{F}(\mathbf{X})$ is computed by taking $\mathcal{G} = \mathcal{F}^2$ in Eq. (B3)

$$\mathbb{E}_{\zeta}[\mathcal{F}(\mathbf{X})^2] = \mathcal{F}(\mathbf{x})^2 + \frac{1}{2S} \sum_{j,j'}^K \frac{\partial^2 (\mathcal{F}(\mathbf{x})^2)}{\partial z_j \partial z_{j'}} \boldsymbol{\Sigma}_{jj'} + o\left(\frac{1}{S}\right).\tag{B7}$$

We need to expand the term $\frac{1}{2} \frac{\partial^2 (\mathcal{F}(\mathbf{x})^2)}{\partial z_j \partial z_{j'}}$:

$$\frac{1}{2} \frac{\partial^2 (\mathcal{F}(\mathbf{x})^2)}{\partial z_j \partial z_{j'}} = \frac{\partial}{\partial z_{j'}} \left(\mathcal{F}(\mathbf{x}) \frac{\partial \mathcal{F}(\mathbf{x})}{\partial z_j} \right) = \frac{\partial \mathcal{F}(\mathbf{x})}{\partial z_j} \frac{\partial \mathcal{F}(\mathbf{x})}{\partial z_{j'}} + \mathcal{F}(\mathbf{x}) \frac{\partial^2 \mathcal{F}(\mathbf{x})}{\partial z_j \partial z_{j'}}.\tag{B8}$$

Hence, the covariance of $\mathcal{F}(\mathbf{X})$ is

$$\begin{aligned}\text{Cov}[\mathcal{F}(\mathbf{X})] &= \mathbb{E}[\mathcal{F}(\mathbf{X})^2] - \mathbb{E}[\mathcal{F}(\mathbf{X})]^2 \\ &= \frac{1}{S} \sum_{j,j'} \left(\frac{\partial \mathcal{F}(\mathbf{x})}{\partial z_j} \frac{\partial \mathcal{F}(\mathbf{x})}{\partial z_{j'}} + \mathcal{F}(\mathbf{x}) \frac{\partial^2 \mathcal{F}(\mathbf{x})}{\partial z_j \partial z_{j'}} \right) \boldsymbol{\Sigma}_{jj'} - \frac{1}{S} \mathcal{F}(\mathbf{x}) \sum_{j,j'} \frac{\partial^2 \mathcal{F}(\mathbf{x})}{\partial z_k \partial z_{j'}} \boldsymbol{\Sigma}_{jj'} + o\left(\frac{1}{S}\right) \\ &= \frac{1}{S} \sum_{j,j'} \frac{\partial \mathcal{F}(\mathbf{x})}{\partial z_j} \frac{\partial \mathcal{F}(\mathbf{x})}{\partial z_{j'}} \boldsymbol{\Sigma}_{jj'}(\theta) + o\left(\frac{1}{S}\right).\end{aligned}\tag{B9}$$

3. Higher order cumulants

The M -th order cumulants can be written as

$$\kappa_M(\mathcal{F}(\mathbf{X})) = \sum_{\pi = \{(m_l, n_l)\}} (|\pi| - 1)! (-1)^{|\pi|-1} \prod_l \mathbb{E}[\mathcal{F}(\mathbf{X})^{m_l}]^{n_l},\tag{B10}$$

where $\pi = \{(m_l, n_l)\}$ is a partition of $[M] := \{1, 2, \dots, M\}$ where there are n_j parts having m_j elements, thus $|\pi| = \sum_l n_l$.

First of all, by taking $\mathcal{G} = \mathcal{F}^m$ in Eq. (B3) we have

$$\mathbb{E}[\mathcal{F}(\mathbf{X})^m] = \mathcal{F}(\mathbf{x})^m + \frac{1}{2S} \sum_{j,j'=1}^K \frac{\partial^2(\mathcal{F}(\mathbf{x})^m)}{\partial z_j \partial z_{j'}} \boldsymbol{\Sigma}_{jj'} + o\left(\frac{1}{S}\right), \quad (\text{B11})$$

where

$$\frac{\partial^2(\mathcal{F}(\mathbf{x})^m)}{\partial z_j \partial z_{j'}} = m(m-1)\mathcal{F}(\mathbf{x})^{m-2} \frac{\partial \mathcal{F}(\mathbf{x})}{\partial z_j} \frac{\partial \mathcal{F}(\mathbf{x})}{\partial z_{j'}} + m\mathcal{F}(\mathbf{x})^{m-1} \frac{\partial^2 \mathcal{F}(\mathbf{x})}{\partial z_j \partial z_{j'}}. \quad (\text{B12})$$

Hence,

$$\begin{aligned} \mathbb{E}[\mathcal{F}(\mathbf{X})^m]^n &= \mathcal{F}(\mathbf{x})^{mn} + \frac{mn}{2} \mathcal{F}(\mathbf{x})^{mn-2} \sum_{j,j'} \left((m-1) \frac{\partial \mathcal{F}(\mathbf{x})}{\partial z_j} \frac{\partial \mathcal{F}(\mathbf{x})}{\partial z_{j'}} \right. \\ &\quad \left. + \mathcal{F}(\mathbf{x}) \frac{\partial^2 \mathcal{F}(\mathbf{x})}{\partial z_j \partial z_{j'}} \right) \frac{\boldsymbol{\Sigma}_{jj'}}{S} + o\left(\frac{1}{S}\right), \end{aligned} \quad (\text{B13})$$

By dropping $o\left(\frac{1}{S}\right)$, we get (we use the fact $\sum_l m_l n_l = M$)

$$\begin{aligned} &\prod_j \mathbb{E}[\mathcal{F}(\mathbf{X})^{m_l}]^{n_l} \\ &= \mathcal{F}(\mathbf{x})^{\sum_l m_l n_l} + \frac{\mathcal{F}(\mathbf{x})^{\sum_l m_l n_l - 2}}{2} \sum_{j,j'} \left(\left(\sum_l m_l (m_l - 1) n_l \right) \frac{\partial \mathcal{F}(\mathbf{x})}{\partial z_j} \frac{\partial \mathcal{F}(\mathbf{x})}{\partial z_{j'}} \right. \\ &\quad \left. + \left(\sum_l m_l n_l \right) \mathcal{F}(\mathbf{x}) \frac{\partial^2 \mathcal{F}(\mathbf{x})}{\partial z_j \partial z_{j'}} \right) \frac{\boldsymbol{\Sigma}_{jj'}}{S} \\ &= \mathcal{F}(\mathbf{x})^M + \frac{\mathcal{F}(\mathbf{x})^{M-2}}{2} \sum_{j,j'} \left(\left(\sum_l m_l (m_l - 1) n_l \right) \frac{\partial \mathcal{F}(\mathbf{x})}{\partial z_j} \frac{\partial \mathcal{F}(\mathbf{x})}{\partial z_{j'}} \right. \\ &\quad \left. + \left(\sum_l m_l n_l \right) \mathcal{F}(\mathbf{x}) \frac{\partial^2 \mathcal{F}(\mathbf{x})}{\partial z_j \partial z_{j'}} \right) \frac{\boldsymbol{\Sigma}_{jj'}}{S}. \end{aligned} \quad (\text{B14})$$

Now we use the identities

$$\sum_{\pi=\{(m_l, n_l)\}} (|\pi| - 1)! (-1)^{|\pi|-1} = 0, \quad (\text{B15})$$

$$\sum_{\pi=\{(m_l, n_l)\}} (|\pi| - 1)! (-1)^{|\pi|-1} \sum_l m_l n_l = \delta_{1M}, \quad (\text{B16})$$

$$\sum_{\pi=\{(m_l, n_l)\}} (|\pi| - 1)! (-1)^{|\pi|-1} \sum_l \frac{m_l (m_l - 1) n_l}{2} = \delta_{2M}, \quad (\text{B17})$$

we obtain that all term in Eq. (B10) vanishes other than $o\left(\frac{1}{S}\right)$, and therefore $\kappa_M(\mathcal{F}(\mathbf{X})) = o\left(\frac{1}{S}\right)$ for all $M \geq 3$.

Appendix C: Post-reservoir Loss Function

In this section, we provide a general formalism to analyze the post-reservoir loss function, and explicitly show that the post-reservoir loss in Eq. (12) is approximately Gaussian, that is $\hat{L}(\boldsymbol{\theta}) \sim \mathcal{N}(\mu(\boldsymbol{\theta}), s(\boldsymbol{\theta}))$ where $\mu(\boldsymbol{\theta})$ and $s(\boldsymbol{\theta})$ to be determined.

To simplify the notation in the derivation, we define a loss function $\mathcal{L}(\mathbf{w}, \mathbf{z})$, where \mathbf{z} generically denotes the feature vector. When quantum shot noise is included, we use $\mathbf{z} \leftarrow \mathbf{X}(\mathbf{u})$, and the loss is given by $\mathcal{L}(\mathbf{w}, \mathbf{X}(\mathbf{u}))$. There is a unique set of weights \mathbf{w}^* s.t.

$$\mathbf{w}^*(\boldsymbol{\theta}) = \operatorname{argmin}_{\mathbf{w}} \frac{1}{N} \sum_n \mathcal{L}(\mathbf{w}, \mathbf{X}(\mathbf{u}^{(n)})). \quad (\text{C1})$$

This is equivalently solved by equations

$$\sum_{n'} \frac{\partial \mathcal{L}}{\partial w_j}(\mathbf{w}^*, \mathbf{z}^{(n')}) = 0, \quad (\text{C2})$$

by substituting $(\mathbf{z}^{(1)}, \dots, \mathbf{z}^{(N)}) \leftarrow (\mathbf{X}(\mathbf{u}^{(1)}), \dots, \mathbf{X}(\mathbf{u}^{(N)}))$. It gives a natural definition of an (NK) -variate function $\mathbf{w}^*(\mathbf{z}^{(1)}, \dots, \mathbf{z}^{(N)})$ and

$$\mathcal{L}^*(\mathbf{z}^{(1)}, \dots, \mathbf{z}^{(N)}) = \frac{1}{N} \sum_{n'=1}^N \mathcal{L}(\mathbf{w}^*(\mathbf{z}^{(1)}, \dots, \mathbf{z}^{(N)}), \mathbf{z}^{(n')}). \quad (\text{C3})$$

We notice that $\mathcal{L}^*(\mathbf{X}(\mathbf{u}^{(1)}), \dots, \mathbf{X}(\mathbf{u}^{(N)})) = \hat{L}(\boldsymbol{\theta})$ as defined in Eq. (12). Hence in this section, we let function $\mathcal{G} = \mathcal{L}^*$ in Eq. (B3). The underlying random variable is (NK) -variate $(\mathbf{X}(\mathbf{u}^{(1)}), \dots, \mathbf{X}(\mathbf{u}^{(N)}))$, whose second order cumulant is block-wise diagonal:

$$\boldsymbol{\kappa}^{(2)} = \text{diag}\{\boldsymbol{\Sigma}(\mathbf{u}^{(n)})\} = \begin{pmatrix} \boldsymbol{\Sigma}(\mathbf{u}^{(1)}) & \cdots & \mathbf{0} \\ \vdots & \ddots & \vdots \\ \mathbf{0} & \cdots & \boldsymbol{\Sigma}(\mathbf{u}^{(N)}) \end{pmatrix}, \quad (\text{C4})$$

because $\mathbf{X}(\mathbf{u}^{(n)})$ and $\mathbf{X}(\mathbf{u}^{(n')})$ are independent for any $n \neq n'$. Then by applying Eq. (B3), we obtain that $\mathcal{L}^*(\mathbf{X}(\mathbf{u}^{(1)}), \dots, \mathbf{X}(\mathbf{u}^{(N)})) = \hat{L}(\boldsymbol{\theta})$ can be approximated by Gaussian

$$\mathcal{N} \left(\mathcal{L}^*(\{\mathbf{x}(\mathbf{u}^{(n)})\}) + \frac{1}{2S} \sum_{n,j,j'} \frac{\partial^2 \mathcal{L}^*}{\partial z_j^{(n)} \partial z_{j'}^{(n)}} \boldsymbol{\Sigma}_{jj'}(\mathbf{u}^{(n)}), \frac{1}{S} \sum_{n,j,j'} \left(\frac{\partial \mathcal{L}^*}{\partial z_j^{(n)}} \frac{\partial \mathcal{L}^*}{\partial z_{j'}^{(n)}} \right) \boldsymbol{\Sigma}_{jj'}(\mathbf{u}^{(n)}) \right). \quad (\text{C5})$$

Although $\mathcal{L}^*(\mathbf{z}^{(1)}, \dots, \mathbf{z}^{(N)})$ is a highly complex function, within the RGD framework, both $\frac{\partial \mathcal{L}^*}{\partial z_j^{(n)}}$ and $\frac{\partial^2 \mathcal{L}^*}{\partial z_j^{(n)} \partial z_{j'}^{(n)}}$ can be drastically simplified. This follows from the fact that $\mathbf{w}^*(\boldsymbol{\theta})$ minimizes the loss function for fixed internal parameters, $\boldsymbol{\theta}$, and satisfies Eq. (C2)

1. First-order derivative of \mathcal{L}^*

Since $\sum_{n'} \frac{\partial \mathcal{L}}{\partial w_k}(\mathbf{w}^*, \mathbf{z}^{(n')}) = 0$ for all k , we have

$$\begin{aligned} \frac{\partial \mathcal{L}^*}{\partial z_j^{(n)}} &= \frac{1}{N} \left(\sum_{n',k} \frac{\partial \mathcal{L}}{\partial w_k}(\mathbf{w}^*, \mathbf{z}^{(n')}) \frac{\partial w_k^*}{\partial z_j^{(n)}}(\mathbf{z}^{(1)}, \dots, \mathbf{z}^{(N)}) + \frac{\partial \mathcal{L}}{\partial z_j}(\mathbf{w}^*, \mathbf{z}^{(n)}) \right) \\ &= \frac{1}{N} \left(\sum_k \underbrace{\left(\sum_{n'} \frac{\partial \mathcal{L}}{\partial w_k}(\mathbf{w}^*, \mathbf{z}^{(n')}) \right)}_{=0} \frac{\partial w_k^*}{\partial z_j^{(n)}} + \frac{\partial \mathcal{L}}{\partial z_j}(\mathbf{w}^*, \mathbf{z}^{(n)}) \right) \\ &= \frac{1}{N} \frac{\partial \mathcal{L}}{\partial z_j}(\mathbf{w}^*, \mathbf{z}^{(n)}). \end{aligned} \quad (\text{C6})$$

2. Second-order derivative of \mathcal{L}^*

By taking derivative of Eq. (C6) with respect to $z_{j'}$. We notice that

$$\frac{\partial^2 \mathcal{L}^*}{\partial z_j^{(n)} \partial z_{j'}^{(n)}} = \frac{1}{N} \left(\sum_l \frac{\partial^2 \mathcal{L}}{\partial z_j \partial w_l}(\mathbf{w}^*, \mathbf{z}^{(n)}) \frac{\partial w_l^*}{\partial z_{j'}^{(n)}} + \frac{\partial^2 \mathcal{L}}{\partial z_j \partial z_{j'}}(\mathbf{w}^*, \mathbf{z}^{(n)}) \right). \quad (\text{C7})$$

The only unknown quantity $\frac{\partial w_l^*}{\partial z_{j'}^{(n)}}$ is the changing rate of optimal weights with respect to $z_{j'}^{(n)}$. It can be computed by taking derivative of Eq. (C2) with respect to z_j . That is, $\frac{\partial}{\partial z_j^{(n)}} \left(\sum_{n'} \frac{\partial \mathcal{L}}{\partial w_k}(\mathbf{w}^*, \mathbf{z}^{(n')}) \right) = 0$ implies

$$\sum_{n',l} \frac{\partial \mathcal{L}}{\partial w_l \partial w_k}(\mathbf{w}^*, \mathbf{z}^{(n')}) \frac{\partial w_l^*}{\partial z_j^{(n)}} + \frac{\partial \mathcal{L}}{\partial z_j \partial w_k}(\mathbf{w}^*, \mathbf{z}^{(n)}) = 0 \Rightarrow \sum_{j'} \mathbf{H}_{kl} \frac{\partial w_l^*}{\partial z_{j'}^{(n)}} = -\mathbf{K}_{kj}^{(n)}, \quad (\text{C8})$$

where we define $\mathbf{H}_{kl} = \sum_{n'} \frac{\partial^2 \mathcal{L}}{\partial w_k \partial w_l}(\mathbf{w}^*, \mathbf{z}^{(n')})$ and $\mathbf{K}_{kj}^{(n)} = \frac{\partial^2 \mathcal{L}}{\partial w_k \partial z_j}(\mathbf{w}^*, \mathbf{z}^{(n)})$. It is equivalently $\frac{\partial w_l^*}{\partial z_j^{(n)}} = -(\mathbf{H}^{-1} \mathbf{K}^{(n)})_{l,j}$ and thus

$$\frac{\partial^2 \mathcal{L}^*}{\partial z_j^{(n)} \partial z_{j'}^{(n)}} = \frac{1}{N} \left(\frac{\partial^2 \mathcal{L}}{\partial z_j \partial z_{j'}}(\mathbf{w}^*, \mathbf{z}^{(n)}) - (\mathbf{K}^{(n)T} \mathbf{H}^{-1} \mathbf{K}^{(n)})_{j,j'} \right). \quad (\text{C9})$$

Finally, we plug Eq. (C6) and Eq. (C9) into Eq. (C5), and achieves the result the Eq. (C5).

Appendix D: Reservoir gradient-free optimization

As discussed in the main text, jointly optimizing the full sensing pipeline including both the internal parameters of the quantum circuit and the final estimator, presents significant computational challenges due to the high-dimensional, non-convex, and often noisy nature of the optimization landscape. In this section we provide more details on the post-reservoir gradient-free optimization strategy we developed and used to identify the optimal circuit parameters and estimators for the sensing tasks presented in the main text.

Inspired by the DIviding RECTangle (DIRECT) method [57–60] our algorithm strategically selects the evaluation points of the post-reservoir loss function defined as:

$$\hat{L}(\boldsymbol{\theta}) = \min_{\mathbf{w} \in \mathbb{R}^K} \hat{l}(\boldsymbol{\theta}, \mathbf{w}), \quad (\text{D1})$$

which corresponds to Eq. (11) of the main text. Here,

$$\hat{l}(\boldsymbol{\theta}, \mathbf{w}) = \frac{1}{N} \sum_{n=1}^N \mathcal{L}(\mathbf{w}, \mathbf{X}(\mathbf{u}^{(n)})), \quad (\text{D2})$$

is the empirical loss computed with finite samples, N and shots, S . Crucially, for any fixed choice of system parameters $\boldsymbol{\theta}$, the optimization of the linear estimator weights, \mathbf{w} , is convex allowing for efficient computation. To guide the selection of the evaluation points, the algorithm maintains an internal representation of the objective loss function in the form of a surrogate model. Specifically, we employ a Gaussian process (GP) metamodel which provides both a predictive mean and an uncertainty estimate over the objective function. Such probabilistic framework enables informed exploration of the parameter space by balancing exploitation of low-loss regions and exploration of uncertain areas, thereby improving sample efficiency during optimization. At each optimization step, the next evaluation point is selected based on a scoring criterion that combines both exploration and exploitation. This score is constructed using the predictive mean and variance of the GP metamodel, with tunable weights that control the relative importance of these two objectives. Importantly, these weights can be adapted dynamically across epochs, allowing the algorithm to emphasize exploration in the early stages and gradually shift toward exploitation as convergence is approached.

For the successful implementation of a metamodel-based optimization approach, it is essential to select a surrogate ansatz that offers sufficient flexibility while capturing the essential features of the loss landscape. The surrogate must be capable of modeling relevant variations in the objective function across the parameter space without overfitting to noise or sparse observations. In our case, the hyperparameters of the Gaussian process metamodel are determined via maximum-likelihood estimation, ensuring that the model remains well-calibrated to the observed data throughout the optimization.

To gain further insight into the structure of the target loss function, we begin by analyzing the behavior of a generic observable \hat{O} as a function of a system parameter θ :

$$g(\theta) = \langle \psi_0 | \mathcal{U}^\dagger(\theta) \hat{O} \mathcal{U}(\theta) | \psi_0 \rangle. \quad (\text{D3})$$

Here, $\mathcal{U}(\theta) = e^{-i\theta\hat{G}}$ denotes a unitary operator generated by the Hermitian operator \hat{G} , and $|\psi_0\rangle$ is the initial state while without loss of generality, we focus on the dependence on a single parameter θ . Since \hat{G} is Hermitian, it can

be diagonalized as $\hat{G} = \sum_j \lambda_j |j\rangle \langle j|$, where $\{\lambda_j\}$ are real eigenvalues and $\{|j\rangle\}$ form an orthonormal eigenbasis. This leads to the decomposition

$$\mathcal{U}(\theta) = \sum_j e^{-i\theta\lambda_j} |j\rangle \langle j|, \quad (\text{D4})$$

and consequently,

$$g(\theta) = \langle \psi_0 | \left(\sum_k e^{i\theta\lambda_k} |k\rangle \langle k| \right) \hat{\mathcal{O}} \left(\sum_l e^{-i\theta\lambda_l} |l\rangle \langle l| \right) | \psi_0 \rangle \quad (\text{D5})$$

$$= \sum_{k,l} c_k^* c_l \langle k | \hat{\mathcal{O}} | l \rangle e^{i\theta(\lambda_k - \lambda_l)}, \quad (\text{D6})$$

where $c_l = \langle l | \psi_0 \rangle$ are the expansion coefficients of the initial state in the eigenbasis of \hat{G} . As a result, $g(\theta)$ can be expressed as a finite Fourier series:

$$g(\theta) = \sum_{m>0} A_m \cos(m\theta) + B_m \sin(m\theta), \quad (\text{D7})$$

where the frequencies m correspond to the distinct values of the eigenvalue differences $\lambda_k - \lambda_l$ of the generator \hat{G} , and the coefficients A_m, B_m depend on the matrix elements of $\hat{\mathcal{O}}$ and the initial state $|\psi_0\rangle$.

If \hat{G} has only two distinct eigenvalues, $+r, -r$, then

$$g(\theta) = A \cos(2r\theta) + B \sin(2r\theta) \quad (\text{D8})$$

and

$$\frac{dg(\theta)}{d\theta} = -2rA \sin(2r\theta) + 2rB \cos(2r\theta). \quad (\text{D9})$$

With some simple algebra it is straightforward to obtain that

$$\frac{dg(\theta)}{d\theta} = \frac{2r}{2 \sin(2s)} \left[g\left(\theta + \frac{s}{r}\right) - g\left(\theta - \frac{s}{r}\right) \right]. \quad (\text{D10})$$

If we choose $s = \pi/4$ then we obtain the parameter- shift rule [63, 64]

$$\frac{dg(\theta)}{d\theta} = r \left[g\left(\theta + \frac{\pi}{4r}\right) - g\left(\theta - \frac{\pi}{4r}\right) \right]. \quad (\text{D11})$$

Finally, this analysis can be extended to cases where the observable is obtained after the application of a sequence of unitary operations, each depending on a different parameter. Specifically, we consider

$$g(\boldsymbol{\theta}) = \langle \psi_0 | \left(\prod_k \mathcal{U}_k^\dagger(\theta_k) \right) \hat{\mathcal{O}} \left(\prod_k \mathcal{U}_k(\theta_k) \right) | \psi_0 \rangle, \quad (\text{D12})$$

which corresponds to the structure of the sensing task discussed in the main text. In such cases, the resulting function $g(\boldsymbol{\theta})$ can be expressed as a product of Fourier series in each parameter:

$$g(\boldsymbol{\theta}) = \prod_i \sum_{m_i} [A_{m_i} \cos(m_i \theta_i) + B_{m_i} \sin(m_i \theta_i)], \quad (\text{D13})$$

where m_i denotes the possible differences between eigenvalues of the generator associated with parameter θ_i .

This functional form highlights that $g(\boldsymbol{\theta})$ resides within a low-bandwidth, structured function space. Therefore, selecting a surrogate model ansatz that reflects this Fourier structure can significantly enhance the efficiency and accuracy of the optimization process. In Fig. 9 we demonstrate the numerical convergence of our algorithm for estimating the unknown parameter u and for a gaussian prior distribution as a function of the number of iterations (epochs). The optimization is initialized within a search region restricted to boxes spanning from 50% to 150% of a preliminary optimal value. This initial estimate is obtained from an extensive exploration of the loss landscape using

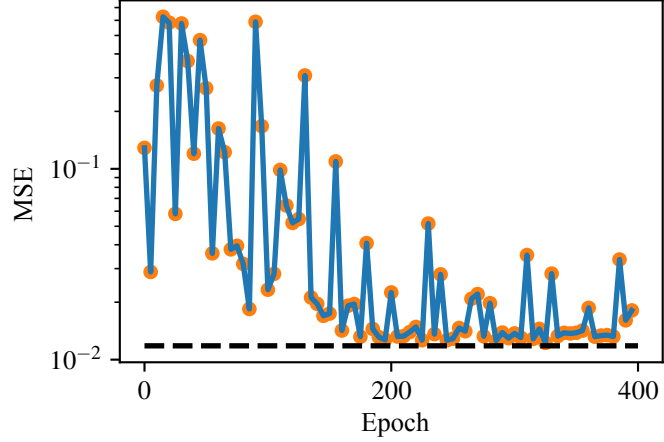


Figure 9. Optimization trajectory. Mean squared error as the number of iteration for finding the optimal circuit and estimator for $n_{\text{en}} = 1, n_{\text{de}} = 2, S = 1$, and $L = 32$ (see main text). The optimization is initialized from a preliminary estimate obtained via Gauss-Hermite quadrature with $n = 75$ points, corresponding to boxes spanning 50% to 150% of the initial optimum leading to a fast convergence. The algorithm is guaranteed to find the optimal solution (shown in black dashed line) since not only exploits promising values of the parameter space but keeps exploring new parts that are less explored. The occasional jumps to higher MSE values arise from mis-approximations of the true loss function by the surrogate model, which are subsequently corrected as the optimization progresses.

Gauss-Hermite quadrature integration, which is applicable in the case of Gaussian prior distributions of the unknown parameter u .

Within this approach, any Gaussian integral of the form $\int_{-\infty}^{\infty} dx e^{-x^2} f(x)$ can be approximated by the Gauss-Hermite quadrature rule

$$\int_{-\infty}^{\infty} dx e^{-x^2} f(x) \approx \sum_{i=1}^n \beta_i f(x_i), \quad (\text{D14})$$

where n denotes the number of quadrature points x_i are the roots of the Hermite polynomial $H_n(x)$ and β_i are the corresponding weights. In the results presented in this work, we fix $n = 75$, which already provides sufficient accuracy while drastically reducing the number of evaluations of the loss function, thereby making the initial search highly efficient.